Superheat Stability of an Evaporator and Thermostatic Expansion Valve

M. J. Lenger, A. M. Jacobi, and P. S. Hrnjak

ACRC TR-138 July 1998

For additional information:

Air Conditioning and Refrigeration Center
University of Illinois
Mechanical & Industrial Engineering Dept.
1206 West Green Street
Urbana, IL 61801

(217) 333-3115

Prepared as part of ACRC Project 76
Superheat Stability of Evaporators and Valves
A. M. Jacobi and P. S. Hrnjak, Principal Investigators

The Air Conditioning and Refrigeration Center was founded in 1988 with a grant from the estate of Richard W. Kritzer, the founder of Peerless of America Inc. A State of Illinois Technology Challenge Grant helped build the laboratory facilities. The ACRC receives continuing support from the Richard W. Kritzer Endowment and the National Science Foundation. The following organizations have also become sponsors of the Center.

Amana Refrigeration, Inc.
Brazeway, Inc.
Carrier Corporation
Caterpillar, Inc.
Copeland Corporation
Dayton Thermal Products
Delphi Harrison Thermal Systems
Eaton Corporation
Ford Motor Company
Frigidaire Company
General Electric Company
Hydro Aluminum Adrian, Inc.
Indiana Tube Corporation
Lennox International, Inc.
Modine Manufacturing Co.
Peerless of America, Inc.
The Trane Company
Whirlpool Corporation
York International, Inc.

For additional information:

Air Conditioning & Refrigeration Center
Mechanical & Industrial Engineering Dept.
University of Illinois
1206 West Green Street
Urbana IL 61801

217 333 3115

ABSTRACT

In some refrigeration applications, difficulties arise in establishing stable evaporator operating conditions, especially when using a thermostatic expansion valve. The unstable superheat signal, sometimes called hunting, of an evaporator was investigated by developing a mathematical model of a thermostatic expansion valve and a two-passage concentric-tube evaporator. The model was then used to study the dynamic response of the evaporator and valve in response to changes in the system operating conditions.

The evaporator model was based on a two-passage concentric-tube heat exchanger configuration. Equations for the conservation of mass, momentum, and energy were used to simulate the flow and heat transfer, where differential equations for the length of the two-phase region and mean void fraction allowed the dynamic behavior of the evaporator to be investigated. The model also has the capability to examine the effects of refrigerant and heat flux maldistribution among the passages.

The thermostatic expansion valve model takes into account the pressure forces on the diaphragm as well as the pressure drop across the orifice when predicting the refrigerant mass flow rate. The geometrical parameters that were varied in this study included the orifice size, obstructing pin-tip angle, and diaphragm area. The model also includes the effects of the spring constant, bulb time constant, and offset temperature—as determined by the force applied by the obstructing pin when the valve is closed.

Superheat response was investigated by imposing suction line pressure oscillations that varied over a range of frequencies. Large superheat fluctuations were found to exist in a given frequency band, where the period was found to be on the order of 50 to 100 seconds, and pressure oscillations in this range should be avoided in operation. Disturbances outside of this frequency band did not produce significant superheat responses. Factors influencing the magnitude of the superheat response depend on the frequency of the perturbations: at high frequencies the valve does not respond to superheat

fluctuations (feedback), but is very sensitive to the slope of the flow rate versus superheat curve as determined by valve geometry; on the other hand, at low frequencies the valve behavior is dominated by the superheat feedback, and the flow rate versus superheat curve is insignificant.

The effect of the valve parameters was also investigated by imposing a step increase of the suction line pressure and simulating the response of the evaporator superheat over time. This approach allowed comparison of the steady-state and transient behavior of superheat with different valve designs.

TABLE OF CONTENTS

Page

LIST OF TABLES

Page

LIST OF FIGURES

Page

NOMENCLATURE

Roman Symbols:

A	area [m^2]
Bo	boiling number, $q''/G\lambda$, [-]
c	specific heat [kJ/kg-K]
Co	convection number [Co]
D	time or spacial derivative of a function
d	diameter [m]
E	energy [J]
Ea	non-dimensional parameter for the slip ratio [-]
Eb	non-dimensional parameter for the slip ratio [-]
e	sum of internal, kinetic, and potential energy [J]
F	force [N]
Fr	Froude number, $G^2/d\rho^2 g$, [-]
FS	constant in calculating the local void fraction [-]
f	friction factor [-]
G	mass flux [kg/m^2-sec]
g	acceleration due to gravity [m/sec^2]
h	convective heat transfer coefficient [W/m^2-K]
i	enthalpy [kJ/kg]
k	spring constant [N/m], thermal conductivity [W/m-K]
L	length [m]
M	mass [kg]
m	mass flow rate [g/sec]

N parameter in calculating the two-phase heat transfer coefficient [-]

Nu Nusselt number, hL_c/k, [-]

P pressure [Pa]

Pr Prandtl number, $\mu c/k$, [-]

Q heat added [J]

q heat rate [W]

q" heat flux [W/m^2]

Re Reynolds number, Gd/μ, [-]

S liquid-vapor slip ratio [-]

T temperature [°C]

t time [sec]

U overall heat transfer coefficient [W/m^2-K]

v velocity [m/sec]

$\forall$ volume [m^3]

W work [J]

We Weber number, $G^2d/\sigma\rho$, [-]

Xtt Martinelli parameter for two-phase turbulent-turbulent flow [-]

x quality [-]

y variable being numerically integrated

z evaporator length increment [m]

Greek Symbols:

α void fraction [-], pin tip angle [degrees]

β two-phase density term used in calculating the local void fraction [-]

Γ fluid-dependent parameter used to determine the two-phase pressure drop [-]

δ TXV pin and spring deflection [m]

ε tube roughness [-]

ϕ two-phase multiplier [-]

λ enthalpy of vaporization [kJ/kg]

μ dynamic viscosity [kg/m-sec]

ξ non-dimensional length, z/L_{tp}, [-]

ρ density [kg/m^3]

σ surface tension [N/m]

τ bulb time constant [sec]

Ψ two-phase convection coefficient ratio, h/h_l, [-]

Subscripts:

1 evaporator passage one

2 evaporator passage two

acc acceleration

air air

b thermostatic expansion valve bulb

bs bubble suppression

c critical, charactaristic

cb convective boiling

cl closed

cond	condenser
cont	contact
cs	control surface
cv	control volume
d	Darcy
diaph	expansion valve diaphragm
e	exit
evap	evaporator
fg	fluid-to-vapor
frict	friction
i	inlet
initial	initial
l	liquid
LMTD	log-mean temperature difference
lo	liquid-only
local	local
max	maximum
mid	two-phase - superheat boundary
mom	momentum
n	normalized
nb	nucleate boiling
o	outlet
offset	offset
orif	orifice
pp	peak-to-peak
r	refrigerant
ratio	quality ratio per evaporator passage

ref	reference
rm	ambient room
s	superheat
sat	saturation
screw	thermostatic expanion valve screw for deflecting the spring
sl	suction line
sp	spring
store	storage term in a control volume
sur	surface
tot	total
tp	two-phase region
TXV	thermostatic expansion valve
v	vapor
w	water
wall	evaporator wall

overbar indicates spatially-averaged variable

CHAPTER 1 - INTRODUCTION

1.1 Background

In vapor compression systems, there are two opposing factors important in optimizing the performance of the evaporator. For higher effectiveness, the region of two-phase flow should occupy most of the evaporator, giving increased heat transfer on the refrigerant side. On the other hand, if the two-phase region gets near the exit of the evaporator and the system does not have an accumulator, liquid droplets could enter the suction line and damage the compressor. Most refrigerant evaporators operate with 4-5°C superheat at their exits, utilizing most of the evaporator for high heat transfer but still keeping a margin of safety to assure that thermal non-equilibrium and the random behavior of the flow do not cause liquid to enter the compressor.

Many refrigeration cycles use a thermostatic expansion valve (TXV) to control the amount of refrigerant going into the evaporator. A thermostatic expansion valve indirectly senses the evaporator exit superheat and adjusts the inlet flow rate accordingly. Valve manufacturers and operators of refrigeration systems sometimes experience trouble when the expansion valve can not find a steady operating point; the valve alternately opens and closes without reaching a steady set point. This unstable behavior is sometimes called hunting. Often, the cause of this instability is not understood and, although there are corrective measures that can be implemented, most of these measures decrease the efficiency of the system.

The goal of this project was to develop a better understanding of superheat stability. This goal was pursued through the development of a mathematical model simulating the dynamic behavior of an evaporator and thermostatic expansion valve. The influence of valve design and suction-line pressure perturbations were examined to understand the effect on the superheat signal. The valve could be modified by changing the bulb time constant, orifice area, pin tip angle, spring constant, diaphragm diameter, and the spring force on the

closed valve. The pressure perturbations included oscillating the suction-line pressure at various frequencies, as well as looking at the superheat response to a step increase in the suction-line pressure. Understanding evaporator dynamics and how the expansion valve uses feedback to regulate the flow rate may lead to an understanding of why expansion valves hunt.

1.2 Literature Review

1.2.1 Background

There has been a lot of theoretical and computational research directed toward understanding evaporator dynamics and instabilities. In order to understand the stability of an evaporator, a good model is needed to describe the dynamics. Wang and Touber [1] present a summary of several methods to model evaporators, with the three most common being described below.

First, there is the black-box model where components are described only by input-output relationships. This method of analysis uses control theory to characterize stability and understand what feedback is involved. Transfer functions are used to predict the system response to changes in operating conditions, where the transfer functions are found through experimental investigations. Because black-box modeling only uses input-output relationships, this technique is generally the simplest to develop. On the other hand, the physics of the system is lost in the analysis, making it difficult to truly understand what is happening.

Second, there are the two-zone models that generally use a lumped-parameter approach. The evaporator is divided into regions of two-phase flow and superheat, where the conservation equations can be applied to each region separately. Methods of analysis may vary, but a two-zone model is usually a computationally inexpensive way to grasp the basic physical behavior of a system. Some problems with using a two-zone model are that

the local behavior of the system is lost, and that some of the variables in a region, such as the convection coefficient and void fraction, need to be spatially averaged for the analysis.

Third, there are distributed models which discretize the evaporator into many small control volume segments, much like a finite-volume CFD analysis. Distributed models can potentially be more accurate than the two-zone models because of their ability to predict local behavior if the constitutive relations and correct flow regimes are known. A problem with distributed models is that the analysis can become very complex, requiring much more computer time than the two-zone models.

1.2.2 Black-box, or control theory models

Stoecker [2] was one of the first to study the problem of evaporator and expansion valve instabilities. He approached the problem by looking for feedback loops where a generated disturbance will propagate through a system and create a new disturbance when it reaches the exit; this is accomplished by the output response lagging the input by 360°. If the new disturbance has an amplification less than one, the new disturbance will be less than the original disturbance and the effect will gradually disappear. On the other hand, if the amplification is greater than one, the new disturbance will be greater than the original disturbance and the feedback will make operation unstable. Stoecker used a Bode plot to examine the stability of a valve-evaporator system. He observed two things from his analysis: first, an increase in the transport lag will reduce the stability of the system, and second, the time constant describing the thermal capacity of the tube should either be less than 5 seconds or greater than 2 minutes to ensure a stable loop.

Broersen and van der Jagt [3] used an open-loop transfer function to model the dynamics of an expansion valve. They restricted themselves to a single-input single-output feedback consisting of the refrigerant mass flow and the superheat. Broersen's first suggestion to eliminate hunting was to decrease the mass flow rate, thereby increasing the superheat and eliminating exit temperature oscillations. The problem is that decreasing the

flow rate is done at the expense of cooling capacity, reducing the efficiency of the system. He also suggested slowing the bulb transients by increasing the thermal resistance to the bulb, possibly by adding material between the bulb and evaporator. Increasing the resistance poses a problem during start-up though, when the expansion valve needs to respond to transients quickly; at startup a slow bulb response could be dangerous to the system by allowing surges of liquid to exit the evaporator before the valve can sense what is happening. Experimental validation of their resistance theory to eliminate hunting was achieved by putting PVC tape between the bulb and evaporator wall and comparing the response to normal operation.

He, Liu, and Asada [4] developed a mixed lumped-parameter and control theory model to study a vapor compression system. The response of the evaporating pressure, condensing pressure, and superheat due to changes in the compressor speed, fan speed, and expansion valve opening were analyzed. The dynamics of the evaporator and condenser were studied from a transfer function matrix by comparing several input-output pairs. The model was compared to experimental data for small step changes in compressor speed and valve opening. It was found that single-input single-output techniques used for control purposes are insufficient, and they proposed that new multi-input multi-output methods are needed. The authors claim to have developed the first model that can capture the dynamics of the superheat signal in a way that can be used for control design.

1.2.3 Two-zone models

de Bruijn, van der Jagt, and Machielsen [5] created a model to gain insight into hunting by studying the interactions between an expansion valve and evaporator. The effects of two valve parameters were studied: the thermal resistance of the expansion valve bulb and the offset temperature. The effect of the bulb thermal resistance was examined in their model by adjusting the bulb contact area with the evaporator. They concluded from their data that, for a hunting valve, either increasing or decreasing the bulb resistance will

reduce hunting. While increasing the heat resistance gave the most damping, the sluggish response would cause problems during evaporator start-up. Therefore, decreasing the heat resistance was suggested for application.

de Bruijn, van der Jagt, and Machielsen's method of studying the effect of valve static superheat is unclear. They report switching the static superheat from 4.4°C to -2.2°C, but do not report how a negative static superheat was achieved. Therefore, it is not obvious what was done or what level of superheat the bulb was measuring since the evaporating pressures were not given. Nonetheless, the numerical results are in good agreement with the experiment, both showing that the flow rate and exit superheat undergo a sinusoidal response with a period near 145 seconds. The experimental flow rate oscillated between 10.5 and 12.4 g/sec, and the exit temperature fluctuated between 3.2°C and 4.9°C. The magnitude of the superheat and corresponding oscillations were not reported.

Dhar and Soedel [6] created a model of a window air conditioner to understand transients during normal operation. They divided the evaporator into two control volumes, one for the liquid and the other for the vapor, assuming the outlet conditions for each control volume were equal to the bulk conditions within the control volume. Empirical parameters were then combined with the conservation equations for the analysis. They assumed the liquid entering the evaporator separates from the vapor, and then the liquid sits at the bottom of the evaporator coil. As liquid boils, the vapor flows through the evaporator and becomes superheated. Simulations were conducted to study the response of the expansion valve for different values of gain, where the gain is the change in orifice area per change in superheat. They discovered that if the gain is too large the valve will be unstable, but if the gain is too small the system will take a long time to reach its intended operating condition.

Grald and MacArthur [7] also used a lumped parameter approach to modeling an evaporator. They claimed the lumped parameter approach is best suited for simulating system interactions because it avoids the computational intensity of distributed modeling.

They modeled their system by converting the governing equations into two ordinary differential equations that predict the changing length of two-phase flow and vapor density. Grids were then generated to solve for the temperature in both the two-phase and superheat region with an iterative solution technique. The iterations were done as follows: a guess was first made for the evaporator pressure, and once the length of the two-phase region and vapor density differential equations converged, the temperatures and flow rates were calculated. The model was compared to experimental work with inlet flow rate disturbances between 68 and 73 g/sec. They found that the superheat will respond faster to a step decrease in flow rate than it will to a step increase, presumably because when the two-phase length is increasing, the higher tube wall temperature hinders the rate at which the flow will reach steady state.

Wedekind and Kobus [8] used the mean void fraction theory described in Appendix A to study a multi-tube evaporator with thermal and flow maldistribution. The flow asymmetry came from varying the flow rates among the passages, while keeping the inlet qualities for each passage the same. They developed an equivalent single tube model (ESTM) for the system that predicts the transient response of the evaporator by using a weighted average of the individual passages.

1.2.4 Distributed models

Wang and Touber [1] developed a distributed model using PHOENICS, a computer software program. The purpose of the model was to optimize evaporator performance using capacity control. They decided to use a distributed model to gain accuracy, believing that lumped parameter models are inaccurate for direct-expansion evaporators. They presented three sets of results compared against experiments: reaching steady state, responses to different step functions, and operation with on-off cycling. Their model was not compared to experimental data, and no conclusions were presented based on their simulations.

Jia, et al., [9] attempted to improve on Wang and Touber's model by including the effect of refrigerant pressure drop inside the evaporator. They were able to predict the distribution of refrigerant velocity, void fraction, and temperature in space and time, with their focus being the transient response of the superheat to a step change in the inlet flow rate. Comparing a step increase to a step decrease in flow rate showed that the superheat response is faster when the flow is decreasing. They hypothesize that heat stored in the superheat section of the tube affects the time needed for the flow to reach steady-state following an increase in flow. This finding agrees with the two-zone model of Grald and MacArthur.

Gruhle and Isermann [10] developed a distributed parameter model to investigate evaporator superheat stability. Transient responses in a 19.3 m long evaporator were studied as a function of air temperature, condenser pressure, and compressor speed, and the superheat was used as a control variable. Gruhle and Isermann also attempted to explain random fluctuations in the dry-out location. They suggested the random behavior of the two-phase flow length is due to the non-linear behavior of the heat transfer coefficient in the region where the quality is near unity. Even for steady inlet conditions, two-phase flow length oscillations of 5 Hz are predicted for their system by their model.

Nyers and Stoyan [11] also developed a distributed model which included the evaporator, condenser, and expansion valve. Their evaporator was assumed to be a bundle of parallel pipes, 10 m long, and surrounded by flowing water. They assumed the refrigerant was evenly distributed among the tubes and the flow conditions were the same in all pipes. Seemingly, this model could have been simplified into a one-tube model. The authors initially claimed their aim was to vary the control parameters (water temperature, velocity, valve coefficient, compressor speed, condenser pressure) to find a minimum stable superheat, but they did not do so. Instead, they focused on modeling the system response to a 10% sinusoidal oscillation of the condenser temperature. A shortcoming in modeling the expansion valve using only a valve coefficient and pressure difference can be

seen in their plots where the superheat region disappears and liquid exits the evaporator, but the expansion valve model does not respond to any temperature changes or the increased convection coefficient, and the sinusoidal oscillations persist. Although not backed up with experimental results, Nyers and Stoyan suggest their model be used for the investigation of evaporator transients and to verify other control algorithms.

Yasuda, et al. [12] were interested in developing a mathematical model to predict evaporator transients such as hunting. The system model included the compressor, condenser, thermostatic expansion valve, and the evaporator. The expansion valve was modeled assuming a linear relationship between the mass flow rate and superheat, and the maximum flow rate was determined from manufacturer's data. The two-phase refrigerant flow in the evaporator was simplified by using a lumped model, but a distributed model was used in the superheat region. Characteristic values for the evaporator, such as the mean void fraction, local void fraction, and evaporator pressure drop, were determined from both literature and experiments. Yasuda presented three simulations that were compared to experiments. All three simulations started at steady-state, after which the static superheat for the expansion valve was changed. The first change in static superheat was from 8.5°C to 10.5°C, where the refrigerant superheat responded with an asymptotic increase to the new steady-state condition. Changing the static superheat from 10.5°C to 6.5°C resulted in underdamped superheat oscillations, mostly damped out after the first oscillation. The third change in static superheat was from 7.2°C to 3.0°C. This induced signs of hunting, as the superheat temperature was shown to oscillate with no signs of damping.

1.2.5 Experimental investigation

Wedekind [13] investigated transients in fully evaporating refrigerant flow. He used a 30 foot long heated glass tube to observe where refrigerant was last vaporized and how that point moved over time. Wedekind noticed that even when a system is operating at steady inlet conditions, the length of the evaporator occupied by the two-phase region is

continually fluctuating, sometimes up to 10% of the total flow length. It was thought this may be due to liquid slugs being formed upstream and propagating down the tube.

Mumma [14] also investigated flow length oscillations by designing a test evaporator approximately 26 feet long and using thermocouples to measure the tube temperature. Similar to Wedekind, Mumma also noticed that the dry-out point fluctuated during constant inlet conditions. In addition, he found that the random temperature fluctuations at any given point near the end of the two-phase region had completely dissipated by the time they reached the evaporator exit. Mumma proposed that it was only when the two-phase region had random oscillations that exceeded the length of the evaporator that hunting of an expansion valve might result.

Tassou and Al-Nizari [15] presented experimental results to show how the gain of a valve affects both the stability and the energy efficiency of a refrigeration system. Electronic expansion valves were compared to thermostatic expansion valves during both a cold start (after the system has been off a long time) and a hot start (where the compressor is cycled on and off). During a cold start, the thermostatic expansion valve chosen for their experiment was responsible for superheat oscillations from 1°C to 12°C with a frequency of 0.008 Hz. During a hot start, the thermostatic expansion valve induced superheat oscillations from 6°C to 10°C with a frequency of 0.006 Hz.

Hewitt, McMullan, and Moran [16] investigated the stability of plate heat exchangers (PHE) that use a thermostatic expansion valve. They hypothesized that the instabilities in a PHE came from the small channel size. A small channel size could lead to liquid plugs forming and being driven into the suction line by the high vapor velocity. Another potential problem with plate heat exchangers is that the surface disturbances on the plates might lead to greater mist flow, which might cause superheat fluctuations at the evaporator exit from the thermal non-equilibrium. However, during the course of their investigation they did not find their hypotheses to be true. Their experimental work pointed to instabilities at both high and low superheats, where the instabilities at high superheats were attributed to under-

utilization of the expansion valve. They did notice that short bursts of liquid could occasionally be seen in the evaporator outlet, but the effect on stability went unexplained.

Hewitt, et al. also proposed that flow maldistribution among plates might be causing some of the instabilities. They noticed separated flow entering the evaporator and assumed that phase separation occurred when the header supplied refrigerant to the plates. They expressed concern that if the inlet quality were to suddenly increase and vapor was forced into a tube full of liquid, the liquid in that tube would be prematurely pushed out the end by the high vapor velocity. Proposed solutions to valve problems when using plate heat exchangers were to increase the distance from the evaporator exit to the TXV bulb, create a turbulent flow regime in the evaporator inlet, and generate a well-mixed two-phase flow.

Barnhart [17] examined slug formation in an evaporator and related it to the superheat and pressure signal. He confirmed that the formation of a slug will cause a pressure spike in the evaporator, since the slug forces the vapor flow to slow and compress when the vapor flow cross-sectional area is reduced. The pressure spike induced by the slug decreased the pressure drop across the expansion valve (non-thermostatic), leading to small inlet flow oscillations into the evaporator. It should be noted that he found no correlation between the compressor and slug formation since the compressor operates at a frequency of at least 7 Hz, twenty times that of the slug and pressure frequency he observed at 0.35 Hz.

At the exit of the evaporator, Barnhart found superheat fluctuations with the same frequency as the slug formation. Interestingly, the exit temperature stayed constant, implying that the oscillating superheat measurements were only a function of the changing saturation temperature. The fact that the exit temperature is a constant also implies that moderate slug activity is damped out before it reaches the evaporator exit. On the other hand, he observed that if two slugs coalesced into one large slug, that large slug propagated farther down the evaporator and there was a chance liquid droplets would exit the

evaporator. The periods of liquid exiting the evaporator corresponded to large superheat temperature reductions; this is consistent with his calculations showing that an exit quality of 99% will reduce the vapor temperature 3°C to fully vaporize the flow. However, these periods of large slug generation and corresponding superheat reduction were irregular and could not be predicted.

1.2.6 Qualitative solutions to hunting

Najork [18] investigated the dynamic behavior of an evaporator and expansion valve control loop with the intention of finding changes that could be made to expansion valves to increase their stability. He developed a block diagram of the control loop to find the temperature and pressure gain for the expansion valve diaphragm. Although Najork realized the evaporator pressure directly influences diaphragm movement, he neglected the evaporator pressure control loop by assuming evaporator pressure variations are small in comparison to bulb pressure changes.

Najork reports that a refrigeration loop will be stable if the critical gain is not exceeded by the temperature gain—where the critical gain is defined as the ratio of the time constant to dead time. He then suggests several ways to increase valve stability.

- Increase the critical gain

1. Decrease the response time of the valve.

- Decrease the temperature gain

2. Decrease the flow rate versus deflection of the pin.
3. Decrease the lift versus bulb temperature. This is accomplished by either increasing the spring constant or initial force exerted by the spring.
4. Decrease the bulb temperature change for a given change in evaporator superheat, possibly by adding resistance between the bulb and evaporator to damp out rapid bulb temperature oscillations at the evaporator exit.

5. Decrease the change in superheat for a given change in flow rate (a function of the evaporator design).

Schoen [19] discussed hunting problems valve users may encounter during operation. For a valve to hunt there must be fluctuations in either the bulb temperature or fluctuations in the evaporator pressure. The valve has an instantaneous response to the evaporator pressure, in fact, compressor-induced fluctuations as small as 1 psi have been known to cause control problems. However, Schoen stated that most hunting problems are the result of the bulb temperature fluctuating. He listed six potential problems that may induce bulb temperature fluctuations.

1. Bulb location. If not correctly placed on the evaporator, the bulb may measure the oil temperature or pools of liquid that collect and get washed away.
2. Load maldistribution. Air-side flow maldistribution may give the evaporator unbalanced heat transfer. The different evaporating rates among passages may lead to the bulb sensing different superheats.
3. Refrigerant maldistribution. Similar to load maldistribution, refrigerant maldistribution may also lead to different superheats being sensed by the bulb at the evaporator exit.
4. Low refrigerant velocity. Low velocity may lead to separated flow where, depending on the evaporator geometry, it is possible the liquid refrigerant may pool up. If enough liquid becomes trapped in the evaporator a flow excursion is possible, leading to a sudden decrease in exit superheat.
5. Maintenance of the valve. If the valve is not properly cleaned, foreign material may affect how the valve behaves.
6. Valve size. Schoen places valve sizing last on the list of causing hunting problems. He stated it is possible for an oversized valve to magnify hunting, but the underlying cause of hunting can normally be attributed to something else.

1.2.7 Chaos

The non-linear behavior of two-phase flow through an evaporator may have some interesting consequences. It is possible that the instabilities seen in evaporating flow are chaotic in nature. Lahey, et al. [20] analyzed the evaporator stability problem by developing a lumped parameter model to study density wave instabilities and looking for chaos in the system. Differential equations were used for the inlet velocity, exit density, boiling boundary, and a length representing the mid-point enthalpy for the liquid single-phase region. Their model assumed sub-cooled liquid enters the evaporator as single-phase and exits the evaporator as two-phase fluid. Lahey and co-workers found bifurcations and a strange attractor for low Froude numbers in a boiling channel. The chaotic behavior was caused by the boiling boundary approaching the end of the evaporator which caused the inlet velocity to decrease.

1.2.8 Shortcomings

Past work in evaporator modeling needs to be improved in several ways. First, there are few multi-passage models available for understanding evaporators. As more applications begin to use plate heat exchangers, dynamic multi-passage evaporator models are needed to accurately predict system behavior. In these multi-passage evaporator models, flow maldistribution also needs to be taken into account. This did not need to be addressed for single-passage evaporators, but multi-passage evaporators experience quality maldistribution and different levels of superheat at the evaporator exit. More evaporator models also need to be developed that can simulate liquid exiting the evaporator. Having liquid enter the suction line can damage the compressor, yet few models can support the transition from an exit superheat to an exit quality.

Investigations into hunting also need to be further refined. Many simulations making use of a thermostatic expansion valve have not considered the important valve parameters. For example, few expansion valve models have included the effects of bulb

and evaporator pressure on the diaphragm. Instead, some rely only on an orifice equation to predict the flow rates into the evaporator, only taking into account the pressure drop across the orifice and neglecting how geometry affects the valve dynamics. Lastly, the underlying cause of hunting needs to be identified. Suggestions have been made to minimize the valve response to certain conditions, but without understanding the physics and dynamics of the system it is difficult to determine the most efficient way to solve the hunting phenomenon.

1.3 Flow Instabilities

Two-phase flow instabilities have been studied extensively in the nuclear industry. Because some of the nuclear applications are slightly different from the refrigeration industry, not all the results can be directly used. For example, most of the flows in nuclear evaporators are always in the two-phase region and no superheat is encountered. In any case, some instabilities encountered by the nuclear industry may lead to an understanding of expansion valve hunting. A detailed analysis of flow instabilities can be found in literature [21] [22] [23] [24] [25], so only a brief summary of the most important will be given.

Instabilities can be classified as being either static or dynamic. Static instabilities can be analyzed using steady-state laws and occur when a perturbation leads from one steady-state operating point to another steady-state operating point. The most well known of these is a flow excursion, or the Ledinegg instability. On the other hand, dynamic instabilities need the full transient equations in order to be correctly modeled. Steady-state equations are not sufficient for dynamic instabilities because feedback is involved, as is the delay time of a propagating wave. The best known and most prevalent dynamic instabilities are the pressure drop and density wave instability.

1.3.1 Ledinegg instability

A flow excursion, or Ledinegg instability [26], will occur when the channel (internal) pressure drop versus flow rate curve is smaller than the supply (external) pressure drop versus flow rate curve, as shown in Equation 1.1. Increasing the flow rate may decrease the internal pressure drop if the flow regime undergoes a transition, such as slug flow becoming annular flow.

$$\left.\frac{\partial(\Delta P)}{\partial G}\right|_{int} < \left.\frac{\partial(\Delta P)}{\partial G}\right|_{ext} \tag{1.1}$$

If the pressure drop versus flow rate curves for a system are similar to those shown in Figure 1.1, a flow excursion is possible. Point "A" is an unstable operating point because the internal pressure drop slope is less than the external pressure drop slope. A small increase in the pressure drop will drive the system to operate at "B", and a flow excursion decreases the mass flow rate of the system. On the other hand, if there is a small pressure drop decrease when operating at point "A", the system will accumulate mass until it reaches steady state at point "C". Both points "B" and "C" are steady operating points because the internal pressure drop is greater than the external pressure drop. Any minor perturbation will drive the system back to where it started.

1.3.2 Pressure drop instability

Because a pressure drop instability is dynamic, transient equations need to be used to solve for the system response. Instead of a one-time flow excursion to a new steady-state, there may be repeated cycling of the flow rate. If an evaporating system has an accumulator or a volume large enough where liquid accumulation may occur, similar to Figure 1.2, then a pressure drop instability may occur. The condenser (P_i) and compressor (P_e) pressures are assumed to be constant, while the pressure inside the accumulator (P_{acc}) is allowed to vary. The mass flux is calculated entering both the accumulator (m_1) and evaporator (m_2).

Figure 1.3 shows both an internal and external pressure drop versus mass flux curve and how the flow rate might cycle. If the system is operating at point "A", a small increase in the accumulator pressure would lead to an increase in the pressure drop across the evaporator. This would cause the flow rate into the accumulator (m_1) and evaporator (m_2) to both decrease, but the flow into the evaporator (m_2) decreases faster. Therefore, more liquid is entering the accumulator than exiting and the pressure inside will increase. This drives the system to point "B" where the pressure inside the accumulator builds. When the accumulator reaches a critical pressure, the accumulator will purge itself and drive the system to point "C". As no steady-state conditions can be found (curve intersections), the cycle continues and the flow rate goes from (B-C-D-E-B).

1.3.3 Density wave instability

The most common dynamic instability is the density wave oscillation, where information about the exit conditions is propagated back upstream in the form of pressure waves. The period of these oscillations is usually one to two times the time it takes for a particle in the flow to travel the length of tube [24]. Figure 1.4 shows what the evaporating system might look like, where the condenser (P_i) and suction-line (P_e) pressure is held constant and the pressure at the evaporator entrance (P_o) is allowed to fluctuate. If a perturbation of low density two-phase fluid passes through the exit, the exit restriction pressure drop will decrease. This exit pressure drop decrease will propagate upstream to decrease the evaporator pressure drop (P_o-P_e). A smaller evaporator pressure drop will, in turn, increase the pressure drop across the inlet valve (P_i-P_o) inducing an increase in the flow rate. At a time Δt later, the increased flow acting as a density wave will reach the exit and increase the exit restriction pressure drop. A rise in (P_o-P_e) will propagate back upstream to the inlet to decrease the flow rate, hence the oscillations become self-sustained.

1.4 Project Objectives

The objective of this project was to identify and understand the main causes of superheat instability associated with refrigerant evaporators. This goal was pursued through the development of a computer model to study instabilities within an evaporator. The effects of pressure oscillations in the compressor and the characteristics of the expansion valve were examined to determine the onset conditions of superheat instability and how the system responds for various changes in the thermostatic expansion valve design.

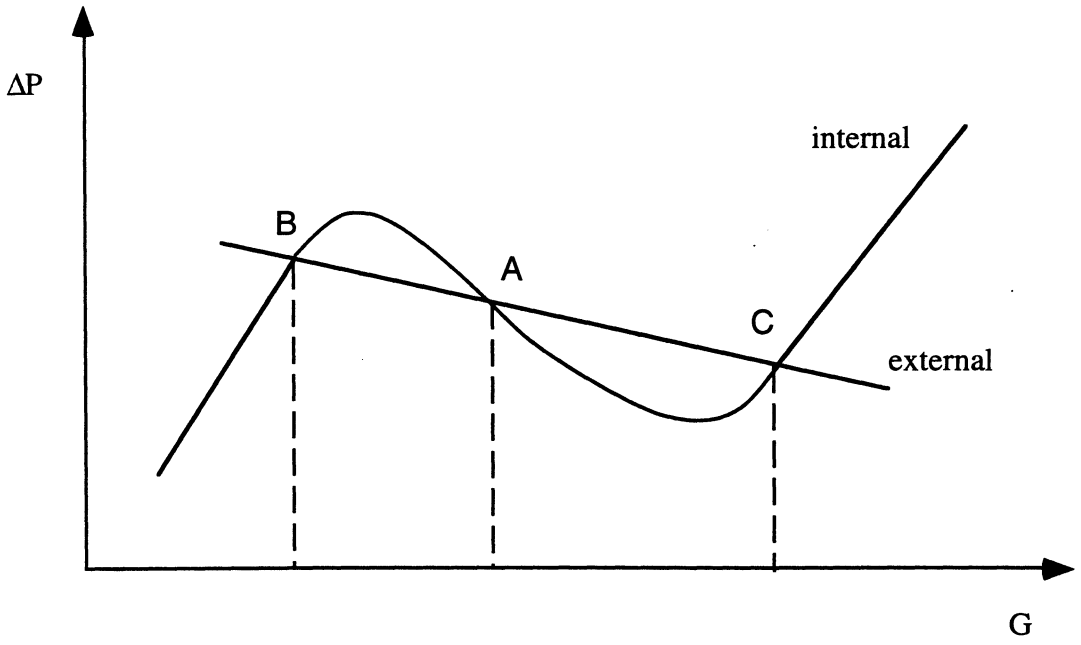

Figure 1.1 Possible system pressure drop vs. flow rate curves. Point "A" is an unstable operating point because the internal pressure drop gradient is less than the external pressure drop gradient. A pressure perturbation causes a Ledinegg instability, driving the flow to points "B" or "C".

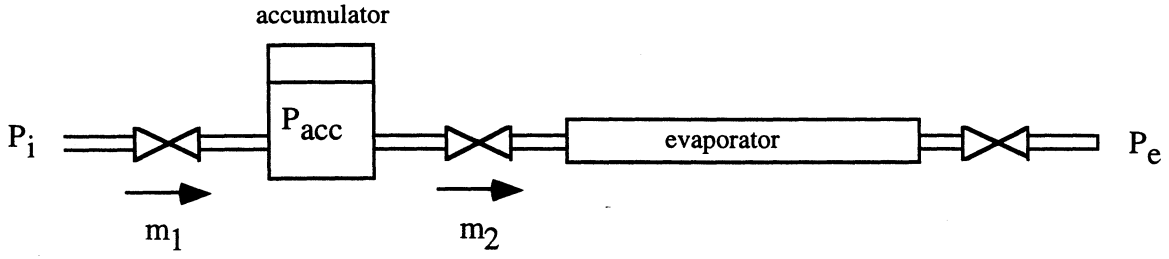

Figure 1.2 Schematic of a system that could encounter a pressure drop instability. Inlet (P_i) and exit (P_e) pressures are held constant while the accumulator pressure (P_{acc}) is allowed to fluctuate. Differences in flow rate between m_1 and m_2 cause mass accumulation or depletion in the accumulator.

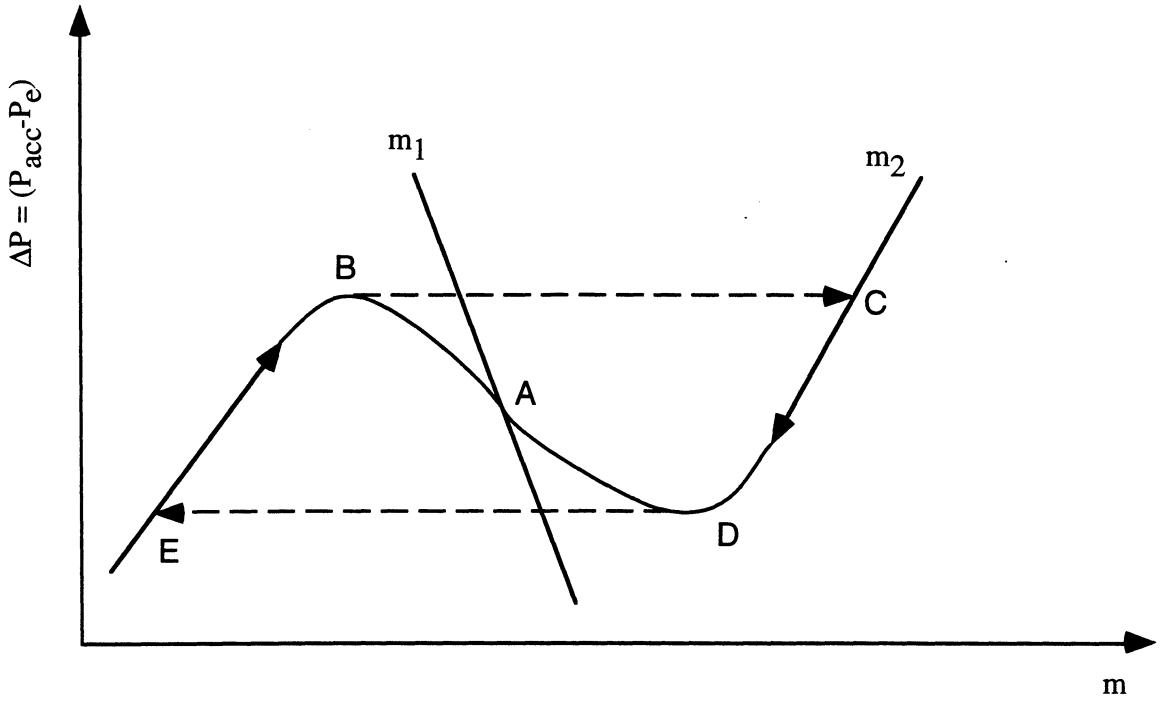

Figure 1.3 Possible system pressure drop vs. flow rate curves. A pressure drop instability may result when operating at point "A". A pressure increase would drive the flow to point "B", and then along the internal pressure drop curve B-C-D-E-B trying to reach steady-state.

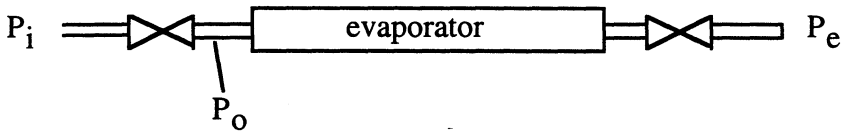

Figure 1.4 Schematic of a system that could encounter a density wave instability. Inlet and exit pressures are held constant while the pressure at the evaporator inlet is allowed to fluctuate. Pressure waves generated at the evaporator exit propagate through the system which change the flow rate through the expansion valve.

CHAPTER 2 - EVAPORATOR MODEL

2.1 Model Description

The dynamics of an evaporator can be simulated using the computer program developed. The model considers an evaporator with refrigerant flowing through parallel round tubes; each of these round tubes is within another tube, forming a concentric-tube heat exchanger for each pass in the evaporator. Refrigerant flows through the inner tubes, and water is in counterflow through the outer tube concentric annulus. The computer program tracks how the evaporator behaves over time for a prescribed set of conditions and can be used to predict the response of the evaporator to changes in operating parameters. A schematic of the evaporator is shown in Figure 2.1.

Certain parameters are either defined as constants or given a prescribed behavior over time, including the evaporator diameter and length, water-side characteristics, and the pressure boundary conditions. The water-side characteristics of the evaporator need to be known in their entirety; namely, the mass flow rate, inlet temperature, and Nusselt number for the water in each passage of the evaporator need to be prescribed. The Nusselt number for a given geometry can be found in [27], where a table of Nusselt numbers is given for an annulus with several ratios of inner and outer tube diameters. The boundary conditions for the evaporator come from the condenser and compressor. On the condenser side, the temperature and pressure must be given; at the evaporator exit, the suction line pressure must be given. A two-zone method is used in the model, where the principles of conservation of mass, momentum, and energy are applied to a two-phase control volume and a superheat control volume.

2.2 Assumptions

The following assumptions are adopted to simplify the modeling of an evaporator.

1. Time invariant mean void fraction (see Appendix A).
2. Evaporator material has a negligible change in stored energy.
3. Thermal equilibrium in the two-phase and superheat region.
4. One-dimensional flow.
5. Pressure drop in the two-phase region does not affect the saturation temperature as used in calculating the heat transfer.
6. Perfect mixing among passages at the evaporator exit.

2.3 Continuity

The principle of conservation of mass is used to predict how much fluid is in a certain region and how much accumulation or depletion of mass is taking place. Continuity is applied to three control volumes: the inlet header, the two-phase region, and the superheat region. Starting with the integral form of conservation of mass as shown in Equation 2.1, assumptions are made to simplify the equation into a more useful form.

$$\iint_{cs} \rho \bar{v} \cdot d\bar{A} + \iiint_{cv} \frac{\partial \rho}{\partial t} d\forall = 0 \qquad (2.1)$$

2.3.1 Evaporator header region

The first control volume in the evaporator is the header, consisting of the region from the expansion valve to the inlet of the evaporator passages. The header has a constant area, the refrigerant is considered to be incompressible, and it is assumed no accumulation of mass will occur. Therefore, the mass flow rate through the expansion valve must equal the mass flow rate into the evaporator. For a two-passage model, the passage inlet flow rates are related to the flow rate through the expansion valve by Equation 2.2.

$$m_{TXV} = m_{i,1} + m_{i,2} \qquad (2.2)$$

2.3.2 Two-phase region

2.3.2.1 Superheated evaporator

The two-phase region of the evaporator is another control volume. Integrating Equation 2.1 converts the left-hand term into two mass flow rates: one being the flow rate into the evaporator, and the other being the flow rate exiting the two-phase region with respect to the dry-out point. The control volume integral accounts for the rate of change of mass storage from a growing or shrinking two-phase length. After simplification, continuity in the two-phase region when the evaporator has superheat is then written as Equation 2.3.

$$m_i - m_{mid} = \frac{d}{dt} m_{store} \tag{2.3}$$

where

$$m_{store} = \left[\rho_l\left(1-\bar{\alpha}\right) + \rho_v\bar{\alpha}\right] A L_{tp}$$

Because the saturation density, mean void fraction, and cross-sectional area in the mass storage term are time-independent, they can be pulled outside the derivative. Therefore, the differential equation for continuity in the two-phase region is simplified to Equation 2.4.

$$m_i - m_{mid} = \left[\rho_l\left(1-\bar{\alpha}\right) + \rho_v\bar{\alpha}\right] A \frac{dL_{tp}}{dt} \tag{2.4}$$

2.3.2.2 Flooded evaporator

When an evaporator passage does not have a superheat region, continuity in the two-phase region must be written in a different form. The assumption of a time-invariant mean void fraction is no longer applicable when the exit quality changes. Instead of accumulating or depleting mass changing the two-phase length, changes in mass storage now affect the mean void fraction. Equation 2.5 is a modified form of Equation 2.3, with the difference being that the flow rate exiting the control volume is now the flow rate

exiting the evaporator. Equation 2.5 can be simplified to Equation 2.6—the equation used for continuity in the two-phase region without evaporator superheat.

$$m_i - m_o = \frac{d}{dt}\left\{\left[\rho_l\left(1-\bar{\alpha}\right)+\rho_v\bar{\alpha}\right]AL_{tot}\right\} \tag{2.5}$$

$$m_i - m_o = AL_{tot}\left\{\frac{d\rho_l}{dt} - \frac{d}{dt}\left(\rho_l\bar{\alpha}\right) + \frac{d}{dt}\left(\rho_v\bar{\alpha}\right)\right\}$$

$$m_i - m_o = AL_{tot}\left(\rho_v - \rho_l\right)\frac{d\bar{\alpha}}{dt} \tag{2.6}$$

2.3.3 Superheat region

If applicable, the third control volume in the evaporator consists of the superheat region. Similar to Equation 2.3, continuity in the superheat region can be written in terms of the mass flux at the control volume boundaries and the rate of change of stored mass. The flow rate entering the superheat control volume is the same as the flow rate exiting the two-phase region, and the flow rate leaving the control volume is the flow rate exiting the evaporator. Continuity is therefore written as Equation 2.7, and can be simplified to Equation 2.8 by assuming a constant evaporator cross-sectional area superheat vapor density.

$$m_{mid} - m_o = \frac{d}{dt}\left[\rho_v A\left(L_{tot} - L_{tp}\right)\right] \tag{2.7}$$

$$m_{mid} - m_o = -\rho_v A\frac{dL_{tp}}{dt} \tag{2.8}$$

2.4 Conservation of Momentum

Conservation of momentum is applied with an equal pressure drop across the evaporator passages. The general form of the conservation of momentum is given in Equation 2.9; however, application in this form requires information on local density and

velocity that are unavailable for this two-phase flow. Therefore, a simplified approach was adopted.

$$\bar{F} = \frac{d}{dt}(m\bar{v}) = \iint_{cs} \bar{v}\left(\rho \bar{v} \cdot d\bar{A}\right) + \iiint_{cv} \frac{\partial}{\partial t}(\bar{v}\rho)\, d\forall \tag{2.9}$$

The overall evaporator pressure drop is comprised of a two-phase pressure drop and a superheat pressure drop. Furthermore, the two-phase pressure drop may be considered as due to contributions from friction and changes in momentum. Thus, these three pressure drop contributions are added to get an overall pressure drop across the evaporator, as given in Equation 2.10. This approach neglects changes in momentum stored within the evaporator passages.

$$\Delta P_{tot} = \Delta P_{frict} + \Delta P_{acc} + \Delta P_s \tag{2.10}$$

2.4.1 Two-phase region

2.4.1.1 Acceleration pressure drop

In the two-phase region, the acceleration pressure drop is found using a simplified momentum equation where the vapor and liquid velocities are assumed to be uniform in each phase. The correlation was developed by de Souza and Pimenta [28] and is shown in Equation 2.11. The acceleration pressure drop is a function of the refrigerant mass flux and changes in flow quality, void fraction, and density from the inlet to the exit of the two-phase region. The correlation makes use of Zivi's void fraction model [29], where the local void fraction is found from Equation 2.12. If the evaporator has a superheat region, then the exit quality and void fraction are known to be unity, thereby simplifying the acceleration pressure drop to Equation 2.13.

$$\Delta P_{acc} = G^2 \left\{ \left[\frac{x_o^2}{\rho_v \alpha_o} + \frac{(1-x_o)^2}{\rho_l (1-\alpha_o)} \right] - \left[\frac{x_i^2}{\rho_v \alpha_i} + \frac{(1-x_i)^2}{\rho_l (1-\alpha_i)} \right] \right\} \tag{2.11}$$

$$\alpha = \frac{1}{1+\left(\frac{1-x}{x}\right)\left(\frac{\rho_v}{\rho_l}\right)^{0.67}} \tag{2.12}$$

$$\Delta P_{acc} = G^2\left\{\left[\frac{1}{\rho_v}\right]-\left[\frac{x_i^{\,2}}{\rho_v\alpha_i}+\frac{(1-x_i)^2}{\rho_l(1-\alpha_i)}\right]\right\} \tag{2.13}$$

2.4.1.2 Friction pressure drop

The pressure drop due to friction in the two-phase region is found by another correlation proposed by de Souza and Pimenta [28], shown by Equation 2.14. The correlation was developed especially for refrigerant flowing through horizontal straight tubes, and a separated flow model was used.

$$\Delta P_{frict} = \Delta P_{lo}\frac{1}{1-x_i}\int \phi_{lo}^{\,2}\,dx \tag{2.14}$$

In the correlation, ΔP_{lo} is the pressure drop assuming all of the flow is a liquid, calculated as shown below. The two-phase multiplier used in separated flows is defined in Equation 2.15. It is the ratio of the two-phase friction pressure gradient and the pressure gradient that would result if all the flow was liquid. The correlation developed by de Souza found $\phi_{lo}^{\,2}$ to be best approximated by Equation 2.16.

$$\phi_{lo}^{\,2} \equiv \left(\Delta P/\Delta z\right)_{frict} \Big/ \left(\Delta P/\Delta z\right)_{lo} \tag{2.15}$$

$$\phi_{lo}^{\,2} = 1+\left(\Gamma^2-1\right)x^{1.75}\left(1+0.9524\Gamma X_{tt}^{\,0.4126}\right) \tag{2.16}$$

where

$$\Gamma = \left(\frac{\rho_l}{\rho_v}\right)^{0.5}\left(\frac{\mu_v}{\mu_l}\right)^{0.125} \qquad X_{tt} = \left(\frac{1-x}{x}\right)^{0.875}\left(\frac{\rho_v}{\rho_l}\right)^{0.5}\left(\frac{\mu_l}{\mu_v}\right)^{0.125}$$

$$\Delta P_{lo} = 2f_{lo}\frac{L_{tp}}{d}\frac{G^2}{\rho_l} \qquad f_{lo} = \frac{0.079}{Re_{lo}^{0.25}}$$

$$Re_{lo} = \frac{Gd}{\mu_l}$$

2.4.2 Superheat region

In the superheat region, the pressure drop comes only from losses due to friction with the evaporator wall. The correlation used for pressure drop in the superheat region is shown in Equation 2.17, valid for a single-phase fluid in a horizontal pipe with fully developed flow. The Darcy friction factor is calculated using a correlation developed by Churchill [30]; this correlation is valid in all flow regimes, eliminating the need to distinguish between laminar and turbulent flow in the evaporator.

$$\Delta P_s = -f_d\frac{L_s}{d}\frac{G^2}{2\rho_v} \tag{2.17}$$

$$f_d = 8\left[\left(\frac{8}{Re_s}\right)^{12} + \frac{1}{(A+B)^{1.5}}\right]^{1/12} \tag{2.18}$$

where

$$A = \left[2.457\ \ln\frac{1}{\left(\frac{7}{Re_s}\right)^{0.9} + \frac{0.27\varepsilon}{d}}\right]^{16} \qquad B = \left(\frac{37{,}530}{Re_s}\right)^{16}$$

2.5 Conservation of Energy

Conservation of energy is used to relate the rate at which energy is added to the evaporator to the rate at which the refrigerant evaporates or increases in temperature. The full conservation of energy equation is shown in Equation 2.19, and includes heat and

work inputs, as well as the flux across the surface and the rate at which energy is being stored in the control volume. Equation 2.19 can be simplified because an evaporator has no shaft work, and the work done on the boundaries due to tangential stresses can be neglected since it is insignificant when compared to the thermal energy changes. Similar to the simplifications made when integrating the continuity equation, Equation 2.19 can be written in terms of the inlet and exit heat transfer rates, and the rate of energy stored in the control volume. The simplified energy equation in basic form is written as Equation 2.20.

$$\frac{dQ}{dt} + \frac{dW}{dt} = \iint_{cs} e_{tot}\left(\rho \bar{v} \cdot d\bar{A}\right) + \iiint_{cv} \frac{\partial}{\partial t}\left(e_{tot}\rho\right) d\forall \qquad (2.19)$$

$$q_i - q_o = \frac{dE_{store}}{dt} \qquad (2.20)$$

2.5.1 Two-phase region

2.5.1.1 Superheated evaporator

Three sets of equations are used to calculate the heat transfer rate for a control volume. The rate of energy loss of the water is equated to the rate of energy gain of the refrigerant, and the energy transfer constitutive relation closes the equation set.

Water. The heat transfer rate for the water, shown in Equation 2.21, describes the energy loss from the water in the annulus outside the region of refrigerant two-phase flow (see Fig 2.2).

$$q_{tp} = m_w c_w \left(T_{w,mid} - T_{w,o}\right) \qquad (2.21)$$

The steady-state equation is used because the energy storage term is assumed to be negligible. The heat rate for the evaporator is on the order of 400 W and the heat rate from the change in water temperature is on the order of 340 W, however, the rate of energy storage by the water is only about 17 W. Because the heat rate for the evaporator is an

order of magnitude greater than the rate of energy stored in the water, the steady-state equations can be used.

$$q \sim m_r \lambda_{fg} \Delta x \approx (2.5 \text{ g/sec})(200 \text{ J/g})(0.8) \approx 400 \text{ W}$$

$$m_w c_w \Delta T \sim (12 \text{ g/sec})(4 \text{ J/gK})(7 \text{ K}) \approx 340 \text{ W}$$

$$M_w c_w \frac{\Delta T}{\Delta t} \sim (250 \text{ g})(4.2 \text{ J/gK})(1 \text{ K/min}) \approx 17 \text{ W}$$

Refrigerant. The conservation of energy equation used for the refrigerant is Equation 2.22, an expanded form of Equation 2.20. The rate of energy entering the control volume comes from the refrigerant entering the evaporator as well as from the water heat flux, whereas the rate of energy leaving the control volume comes only from refrigerant exiting the end of the two-phase region. Because the saturation properties and mean void fraction are assumed to be constant, Equation 2.23 can be used to calculate the heat transfer rate of the refrigerant in the region of two-phase flow.

$$\left[i_l(1-x_i)+i_v x_i\right]m_i + q_{tp} - i_v m_{tp} = \frac{d}{dt}\left\{\left[\rho_l i_l\left(1-\bar{\alpha}\right)+\rho_v i_v \bar{\alpha}\right]AL_{tp}\right\} \quad (2.22)$$

$$\left[i_l(1-x_i)+i_v x_i\right]m_i + q_{tp} - i_v m_{mid} = \left[\rho_l i_l\left(1-\bar{\alpha}\right)+\rho_v i_v \bar{\alpha}\right]A\frac{dL_{tp}}{dt} \quad (2.23)$$

Rate equation. Lastly, the energy transfer constitutive relation is used, shown in Equation 2.24. The average overall heat transfer coefficient (neglecting storage in the tube material) and the log-mean temperature difference are also defined below.

$$q_{tp} = U_{tp} A_{tp} \Delta T_{LMTD,tp} \quad (2.24)$$

where

$$U_{tp} = \frac{1}{\frac{1}{h_w} + \frac{1}{\bar{h}_{r,tp}}}$$

$$\Delta T_{LMTD} = \frac{\Delta T_o - \Delta T_i}{\ln\left(\frac{\Delta T_o}{\Delta T_i}\right)} \tag{2.25}$$

Because the temperature differences in Equation 2.25 are found at the beginning and the end of the two-phase region, and the water is in counterflow with the refrigerant, ΔT_o and ΔT_i are calculated as:

$$\Delta T_o = T_{w,o} - T_{r,i}$$

$$\Delta T_i = T_{w,mid} - T_{r,i}$$

2.5.1.2 Flooded evaporator

Similar to conservation of mass, the conservation of energy equation for the refrigerant must be written in a different form when an evaporator passage does not have a superheat region. The rate at which energy is accumulating or depleting does not induce a changing two-phase length, but instead changes the mean void fraction. The enthalpy of the refrigerant exiting the evaporator also changes from the enthalpy of saturated vapor to being a function of the exit quality. Therefore, Equation 2.26 is used as a modified form of Equation 2.22. By assuming constant saturation properties, Equation 2.26 can be simplified into Equation 2.27.

$$\left[i_l(1-x_i)+i_v x_i\right]m_i + q_{tp} - \left(i_l + x_o\lambda_{fg}\right)m_o = \frac{d}{dt}\left\{\left[i_l\rho_l\left(1-\bar{\alpha}\right)+i_v\rho_v\bar{\alpha}\right]AL_{tot}\right\} \tag{2.26}$$

$$\left[i_l(1-x_i)+i_v x_i\right]m_i + q_{tp} - \left(i_l + x_o\lambda_{fg}\right)m_o = AL_{tp}\left\{\frac{d}{dt}\left(i_l\rho_l\right) - \frac{d}{dt}\left(i_l\rho_l\bar{\alpha}\right) + \frac{d}{dt}\left(i_v\rho_v\bar{\alpha}\right)\right\}$$

$$\left[i_l(1-x_i)+i_v x_i\right]m_i + q_{tp} - \left(i_l + x_o\lambda_{fg}\right)m_o = AL_{tp}\left(i_v\rho_v - i_l\rho_l\right)\frac{d\bar{\alpha}}{dt} \tag{2.27}$$

The water and rate equations also need to be slightly modified. In place of the water temperature at the refrigerant dry-out point being used ($T_{w,mid}$) in Equation 2.21, it is replaced by the water inlet temperature. Similarly, the log-mean temperature difference in Equation 2.25 also uses the water inlet temperature instead of the temperature at the dry-out point.

2.5.2 Superheat region

In the superheat region, the dynamic storage of energy is assumed to be negligible. This approach is based on the idea that energy addition or depletion due to a changing superheat region is minimal compared to the energy in the two-phase region, an assumption that has also been used by others [1]. The heat transfer rate in the superheat region is found from an energy balance on the water, Equation 2.28, vapor refrigerant, Equation 2.29, and the constitutive equation, Equation 2.30.

$$q_s = m_w c_w \left(T_{w,mid} - T_{w,i}\right) \tag{2.28}$$

$$q_s = m_r c_r \left(T_{r,o} - T_{r,i}\right) \tag{2.29}$$

$$q_s = U_s A_s \Delta T_{LMTD,s} \tag{2.30}$$

where

$$U_s = \frac{1}{\frac{1}{h_w} + \frac{1}{h_{r,s}}}$$

and the log-mean temperature difference defined in Equation 2.25 now uses

$$\Delta T_o = T_{w,mid} - T_{r,i}$$

$$\Delta T_i = T_{w,i} - T_{r,o}$$

2.6 Flow Maldistribution

Because of gravity, inertia, and evaporator geometry, refrigerant flow may not be evenly distributed among a multi-passage evaporator. Maldistribution may lead to some evaporator passages being well utilized and having a high heat transfer rate, while other passages carry mostly vapor and have a low heat transfer rate. In addition to affecting the evaporator performance, maldistribution also causes the evaporator passages to have different levels of superheat when the flow mixes in the suction line. Therefore, understanding the heat transfer effects and superheat response from maldistribution is important when modeling and designing an evaporator.

To allow for flow maldistribution among refrigerant passages, a quality ratio term is prescribed for (n-1) tubes, where n is the number of passages. The quality ratio term defines the percentage of the overall vapor entering a specific passage. Assuming an adiabatic throttling process, the quality entering the evaporator header from the expansion valve can be found from knowing the condenser enthalpy and the evaporator pressure. The evaporator inlet vapor flow rate is found by Equation 2.31. Used in conjunction with conservation of mass, the vapor flow rate distribution between the passages in a two-passage evaporator can be found from Equations 2.32 and 2.33, and the inlet quality for each passage can be found from Equations 2.34 and 2.35.

$$m_{v,i} = x_{TXV} m_{TXV} \tag{2.31}$$

$$m_{v,1} = x_{ratio,1} m_{v,i} \tag{2.32}$$

$$m_{v,2} = m_{v,i} - m_{v,1} \tag{2.33}$$

$$x_{i,1} = \frac{m_{v,1}}{m_{i,1}} \tag{2.34}$$

$$x_{i,2} = \frac{m_{v,2}}{m_{i,2}} \tag{2.35}$$

2.7 Exit Quality in a Flooded Evaporator

If liquid exits an evaporator passage, the two-phase region is no longer a dynamic element—the two-phase region is the length of the evaporator passage. Instead, the dynamic element in the evaporator is the mean void fraction. Because liquid is exiting the evaporator, the actual mean void fraction is smaller than it would be if total evaporation took place, as shown in Equation 2.36. Therefore, if the local void fraction is numerically integrated to the point of complete evaporation (past the evaporator exit), the calculated mean void fraction would exceed the actual value, as shown in Figure 2.3. The length of the evaporator relative to how long the evaporator needs to be to fully vaporize the refrigerant can be found by interpolating between the two integration points where the actual mean void fraction was first exceeded. The exit quality can then be found from Equation C.7, where Appendix C describes the relationship between quality and two-phase length.

$$\overline{\alpha} = \frac{1}{L_{evap}} \int_0^{L_{evap}} \alpha \, dL < \frac{1}{L_{tp}} \int_0^{L_{tp}} \alpha \, dL \tag{2.36}$$

2.8 Two-Phase Convection Coefficient

In order to solve the energy balance in the two-phase region, the average convection coefficient for the refrigerant must be known, where the average convection coefficient in the two-phase region is defined by Equation 2.37. Because the local convection coefficient is a function of quality but needs to be integrated over the two-phase length, the quality needs to be known as a function of two-phase length. Appendix C describes how the correlation was derived to relate the local quality to the normalized two-phase length. Since the local convection coefficient can then be known as a function of spatial coordinates, Equation 2.38 can be used to find the average convection coefficient in the two-phase region.

$$\bar{h}_{tp} \equiv \frac{1}{L_{tp}} \int_0^{L_{tp}} h_{local}(x)\, dL_{tp} \tag{2.37}$$

$$\bar{h}_{tp} = \int_0^1 h_{local}\left(L_{tp,n}\right) dL_{tp,n} \tag{2.38}$$

The local convection coefficient is found using Shah's correlation [31], which makes use of the following non-dimensional parameters:

$$\Psi = \frac{h_{local}}{h_l}$$

$$Co = \left(\frac{1}{x} - 1\right)^{0.8} \left(\frac{\rho_v}{\rho_l}\right)^{0.5}$$

$$Bo = \frac{q''}{G_r \lambda_{fg}}$$

$$Fr_l = \frac{G_r^{\,2}}{d_r \rho_l^{\,2} g}$$

and the liquid convection coefficient, h_l, is calculated by the Dittus-Boelter equation.

$$h_l = 0.023\left[\frac{Gd(1-x)}{\mu_l}\right]^{0.8} Pr_l^{0.4} \frac{k_l}{d} \tag{2.39}$$

Shah classifies the boiling process into four regimes, determined from the parameters above. The first regime is nucleate boiling, which assumes that convection is negligible and heat transfer is determined by the intensity of bubble nucleation. The second regime is called bubble suppression, where both nucleate boiling and convection are significant to the heat transfer. The third regime is pure convective boiling assuming a fully wet surface, and the last regime is pure convective boiling with only a partially wet surface.

Most two-phase convection correlations begin to fail in the dry-out region of the evaporator where mist flow is the primary flow regime. Shah states that his correlation should only be used if the dry-out quality is 80% or higher [32].

The dimensionless parameters are calculated as follows:

$N = Co$	horizontal tubes with $Fr > 0.04$
$N = 0.38\ Co\ Fr^{-0.3}$	horizontal tubes with $Fr < 0.04$
$FS = 14.7$	$Bo > 11e\text{-}4$
$FS = 15.43$	$Bo < 11e\text{-}4$,

$$\psi_{cb} = \frac{1.8}{N^{0.8}}$$

If $N > 1.0$

$$\psi_{nb} = 230\ Bo^{0.54} \quad \text{for} \quad Bo > 0.3e\text{-}4$$
$$\psi_{nb} = 1 + 46\ Bo^{0.54} \quad \text{for} \quad Bo < 0.3e\text{-}4$$

ψ is the larger of ψ_{nb} and ψ_{cb}.

If $0.1 < N < 1.0$

$$\psi_{bs} = FS\ Bo^{0.5} \exp\left(2.74\ N^{-0.1}\right)$$

ψ is the larger of ψ_{bs} and ψ_{cb}.

If $N < 0.1$,

$$\psi_{bs} = FS\ Bo^{0.5} \exp\left(2.47\ N^{-0.15}\right)$$

ψ is the larger of ψ_{bs} and ψ_{cb}.

2.9 Local Void Fraction

The local void fraction is spatially integrated to find the mean void fraction. A correlation by Premoli, et al. [33], usually called the CISE correlation, is used to calculate the local void fraction. This method was chosen because, in calculating the mean density found by $\bar{\rho} = (1-\alpha)\rho_l + \alpha\rho_v$, Whalley [34] found the CISE correlation to be more accurate than the Chisholm, Smith, Zuber, Zivi, or homogeneous models.

The CISE local void fraction is found by Equation 2.40.

$$\alpha = \frac{1}{1+\left(S\frac{1-x}{x}\frac{\rho_v}{\rho_l}\right)} \tag{2.40}$$

where

$$S = 1 + Ea\left(\frac{y}{1+yEb} - yEb\right)^{0.5} \qquad y = \frac{\beta}{1-\beta}$$

$$\beta = \frac{\rho_l x}{\rho_l x + \rho_v(1-x)} \qquad Ea = 1.578\ Re_l^{-0.19}\left(\frac{\rho_l}{\rho_v}\right)^{0.22}$$

$$Eb = 0.0273\ We\ Re_l^{-0.51}\left(\frac{\rho_l}{\rho_v}\right)^{-0.08} \qquad Re_l = \frac{Gd}{\mu_l}$$

$$We = \frac{G^2 d}{\sigma\rho_l}$$

Although the mean void fraction is assumed to be a constant, it actually changes slightly during transients when using Premoli's correlation because it is a function of the mass flux. However, under the mass flow rates experienced by the evaporator, changes in the mean void fraction are small and usually insignificant.

The CISE void fraction correlation requires the surface tension of R-134a. Stegou-Sagia's [35] curve fit to ASHRAE data for R-134a was used, as calculated in Equation 2.41.

$$\sigma = \sigma_{ref}\left(1 - \frac{T}{T_c}\right)^n \tag{2.41}$$

where

$\sigma_{ref} = 0.059893$ N/m

$T_c = 374.18$ K

$$n = 1.2448.$$

2.10 Solution Technique

The computer program used a modified Newton-Raphson method to solve the coupled set of non-linear algebraic and differential equations, summarized in Appendix D. An Adam's integration, described in Appendix B, was then used to solve the transient mass and energy equations. Thus, a quasi-steady solution was obtained for variables such as the evaporator pressure drop, refrigerant mass flow rates, and the refrigerant temperature exiting the evaporator. The transient response was captured by determining the length of the two-phase region in each passage. The two-phase flow region is the length of the evaporator tube occupied by two-phase flow—the rest of the tube length is occupied by super-heated vapor. If the two-phase flow length exceeded the length of the evaporator, liquid was entering the suction line. The governing equations changed as the tube consisted only of two-phase flow and the superheat equations could be neglected. Exit quality then became a new unknown parameter, replacing the refrigerant exit temperature and the other superheat variables.

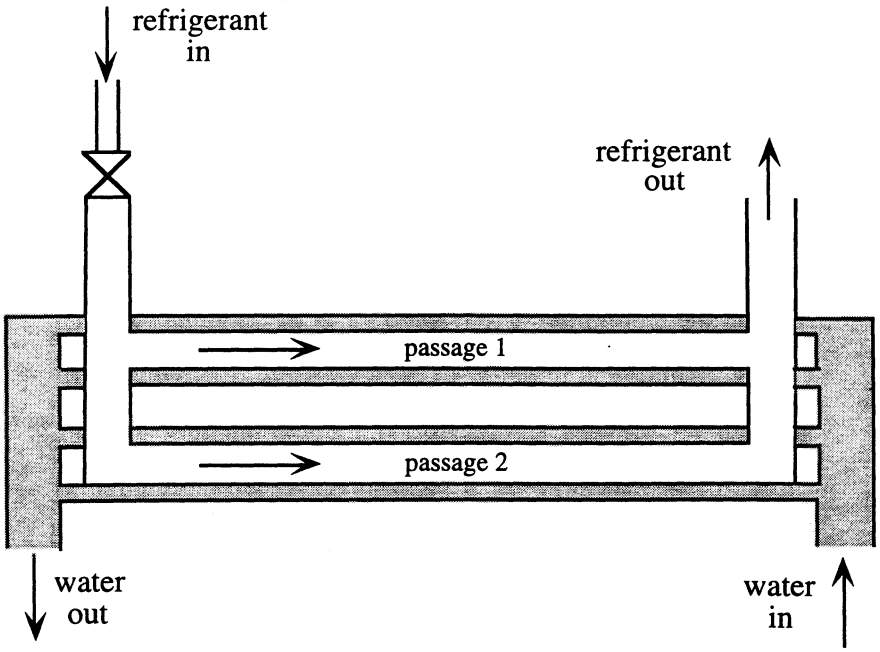

Figure 2.1 Schematic of a two-passage concentric-tube evaporator with water in counterflow to the refrigerant.

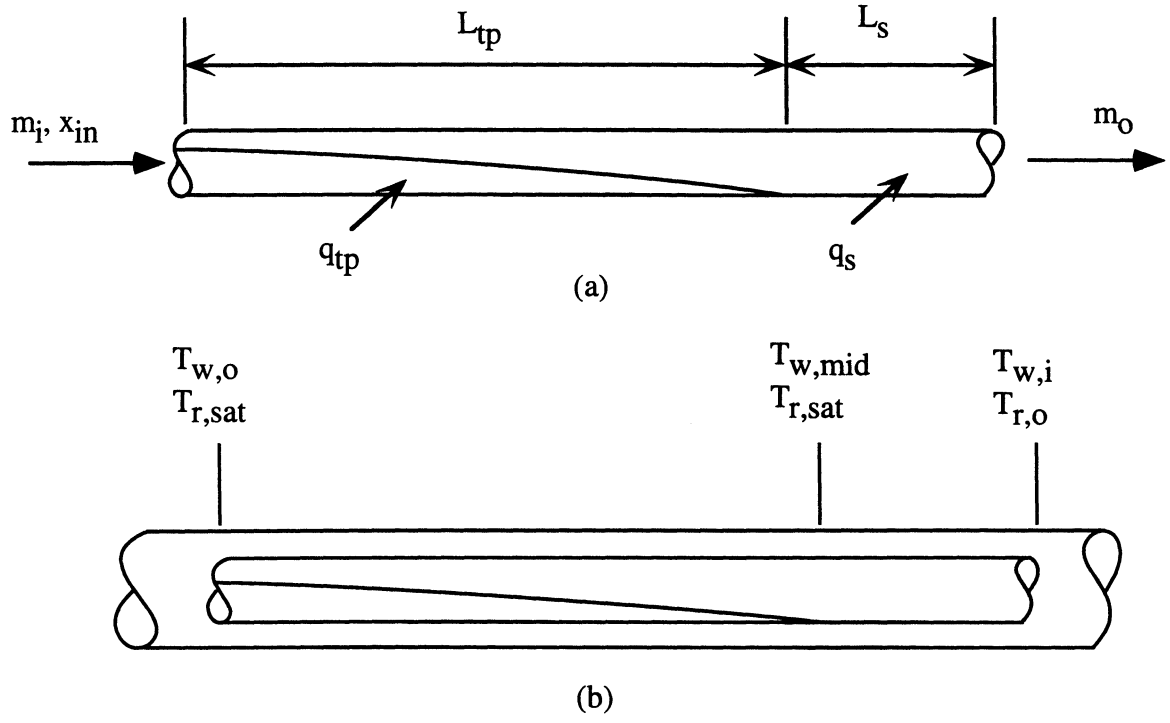

Figure 2.2 (a) Evaporator passage nomenclature and (b) location of the refrigerant and water temperature calculations.

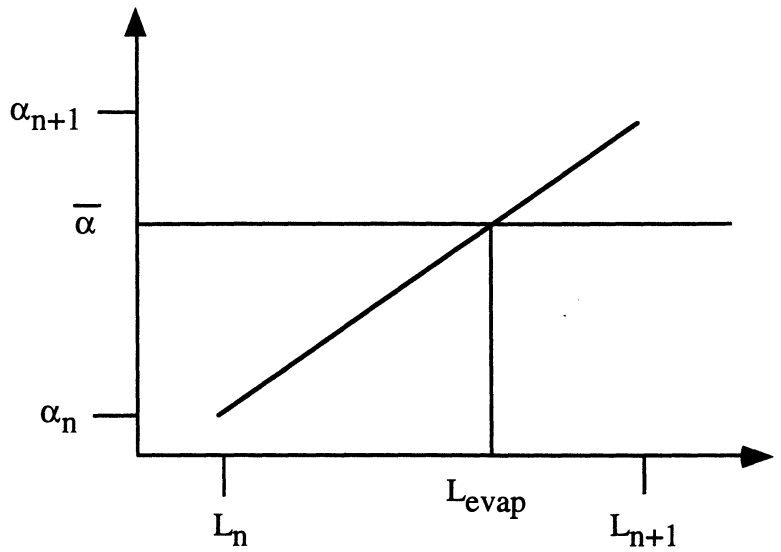

Figure 2.3 When integrated to complete evaporation, the calculated mean void fraction will exceed the actual mean void fraction of the evaporator when the evaporator is flooded. The evaporator length normalized with respect to the length needed to fully evaporate the refrigerant can be found.

CHAPTER 3 - THERMOSTATIC EXPANSION VALVE MODEL

3.1 Expansion Valve Description

A thermostatic expansion valve controls the rate at which refrigerant enters the evaporator. An expansion valve senses the superheat exiting the evaporator and adjusts the refrigerant flow rate, keeping enough superheat to prevent the compressor from taking in liquid. The amount of superheat is measured by attaching a bulb filled with two-phase refrigerant to the exit of the evaporator, with the expectation that the bulb and exiting refrigerant will come into thermal equilibrium. However, the bulb temperature response is slower than the superheat response because of the thermal resistance of the evaporator wall and expansion valve bulb.

Because the bulb always contains a two-phase fluid, changes in the bulb temperature result in changes to the bulb pressure; this pressure is then transmitted to the valve diaphragm to control the valve opening. Resisting the bulb pressure on the diaphragm are the suction-line pressure and the force from a spring under the valve. The spring is adjustable and is used to ensure there is some level of superheat at the evaporator exit before the valve will open. If the evaporator is at a superheat less than the superheat set by the valve, the bulb pressure is not enough to overcome the evaporator pressure and spring. A diagram of the pressures and forces acting within the expansion valve is shown in Figure 3.1.

This level of superheat needed to open the valve is called the offset temperature or the static superheat, and can be controlled by turning a screw that adjusts the spring deflection. Likewise, there is also a superheat that opens the valve to the maximum flow rate (for a given pressure drop across the orifice); when this superheat is reached, the pin is no longer obstructing the orifice and an increase in superheat will not influence the flow rate. Figure 3.2 shows the relationship of the offset temperature, maximum superheat, and maximum mass flow rate on a flow rate versus superheat curve. The shape of the flow rate

versus superheat curve is determined by the valve geometry. Most often, the expansion valve is operating at a superheat somewhere between the offset temperature and maximum superheat. Therefore, if the flow rate versus superheat temperature curve is known, then the flow rate through the valve can be predicted.

3.2 Design Parameters

An expansion valve has certain characteristics that must be known to correctly model its behavior. Previously mentioned was the fact that a two-phase mixture fills the bulb that senses the evaporator superheat. If the operating temperature covers a wide range, some expansion valves will use a mixture of refrigerants to adjust how the bulb pressure responds to different temperatures. However, the current model assumes that pure R-134a is the operating fluid in the bulb. In addition to the bulb fluid characteristics, several physical dimensions and characteristics of the valve need to be prescribed. These are shown in Figure 3.3, and include:

1. Bulb time constant
2. Spring constant
3. Pin tip angle
4. Force the spring exerts on a closed valve
5. Diaphragm diameter
6. Orifice diameter

3.3 Bulb Temperature Response

The bulb temperature response is an important part of the system, and some have pointed to bulb dynamics as a cause of hunting [2] [3] [12] [18] [19]. A bulb will change temperature faster and more accurately measure the evaporator exit conditions if the bulb time constant is decreased.

3.3.1 Lumped capacitance model

The lumped capacitance method is used to predict the transient temperature response of the bulb to changing evaporator exit temperatures. The lumped capacitance method assumes the bulb has an infinite thermal conductivity and is therefore isothermal. The governing equation for the bulb temperature is Equation 3.1, which accounts for heat transfer between the bulb and refrigerant (LHS, first term), heat transfer between the bulb and ambient air (LHS, second term), and the rate of change of the bulb temperature (RHS).

$$h_{r,o}A_{cont}\left(T_{r,o}-T_b\right)+h_{air}A_{b,sur}\left(T_{rm}-T_b\right)=M_b c_b\frac{dT_b}{dt} \qquad (3.1)$$

The lumped capacitance model is accurate only under certain conditions; a Biot number much less than unity is needed before a uniform temperature distribution can be assumed and the lumped capacitance model used [27]. The Biot number, Bi, is defined as

$$Bi \equiv \frac{hL_c}{k}$$

where L_c is the characteristic length. The characteristic length is defined as the ratio of the volume of the solid to the heat transfer surface area.

$$L_c \equiv \frac{\forall}{A_{sur}}$$

Measurements of a representative thermostatic expansion valve were taken to provide sample data. The bulb volume was found to be approximately 11.95 cm^3 and the contact area with the evaporator was estimated to be 1.8 cm^2. Therefore, the characteristic length of this particular bulb was approximately 6.64 cm^2.

If the maximum refrigerant-side convection coefficient is assumed to be 500 W/m^2K, and since the thermal conductivity of copper is approximately 400 W/m-K, then the maximum Biot number expected for this particular bulb would be 0.083. Because Bi << 1.0, the lumped capacitance model can be used.

3.3.2 Experimental results

An experiment was performed where transient temperature measurements of a thermostatic expansion valve bulb were taken. The valve bulb was clamped to the suction line of a refrigeration loop operating at steady-state, where a plate heat exchanger with water in counterflow was used as the evaporator. The evaporator superheat was increased by slowly raising the water inlet temperature from 7.0°C to 12.0°C. Temperatures of the refrigerant, suction-line wall, and expansion valve bulb were measured, with the results shown in Figure 3.4.

3.3.2.1 Refrigerant and air convection coefficients

The refrigerant-side convection coefficient must be known to find the heat transfer rate and bulb time constant. The bulb was placed on a 3/4" diameter tube where the refrigerant flow rate was 42.3 g/sec. The Nusselt number was then found to be approximately 430 and the convection coefficient was approximately 300 W/m^2K. The Biot number for the bulb in this experiment was near 0.05, so the lumped capacitance method was valid.

An important thing to notice from Figure 3.4 is that even at steady-state, the bulb temperature is several degrees higher than the refrigerant temperature. Measurements of a bulb temperature greater than the refrigerant temperature have also been reported elsewhere in literature [6]. The fact that the bulb temperature is several degrees higher than the refrigerant temperature at steady-state can be explained by setting Equation 3.1 equal to zero. Equation 3.1 now shows that the heat transfer between the bulb and refrigerant is balanced by the heat transfer between the bulb and the air. Now, Equation 3.2 can be used to find the air-side convection coefficient on the bulb. The bulb surface area was calculated to be approximately 14.6 cm^2, so the air side convection coefficient in the experiment was approximately 8.2 W/m^2K—a reasonable number for natural convection.

$$h_{air} = \frac{h_{r,o}A_{cont}(T_b - T_{r,o})}{A_{b,sur}(T_{rm} - T_b)} \tag{3.2}$$

3.3.2.2 Bulb time constant

The bulb time constant could also be determined from the experiment. The bulb time constant, τ_b, determines how quickly the bulb temperature will responded to changes in the refrigerant exit temperature. Equation 3.1 can be rearranged into Equation 3.3 to solve for the bulb time constant in terms of variables that have already been measured or calculated on the right-hand-side of the equation.

$$\frac{1}{\tau_b} = \frac{h_{r,o}A_{cont}}{M_b c_b} = \frac{\frac{A_{b,sur}h_{air}(T_{rm} - T_b)}{M_b c_b} - \frac{dT_b}{dt}}{(T_b - T_{r,o})} \tag{3.3}$$

However, in order to solve Equation 3.3 the temperature difference between the bulb and refrigerant needs to be known. Because the experimental data had some scatter, a least-squares curve fit was applied to the refrigerant and bulb temperature response. The polynomial fit to the refrigerant temperature found the response to be approximately

$$T_r = 7.504 + 2.557(10^{-2})t - 4.854(10^{-5})t^2 + 3.137(10^{-8})t^3$$

with R = 0.9993, and the bulb temperature response was approximately

$$T_b = 10.40 - 5.17(10^{-3})t + 1.15(10^{-4})t^2 - 3.67(10^{-7})t^3 + 4.89(10^{-10})t^4 - 2.42(10^{-13})t^5$$

with R = 0.9999.

While the curve fits were very good, there was still some uncertainty in the temperature measurements using the thermocouples. The thermocouple uncertainty for the bulb was assumed to be +0.5 and -0.4°C, and the uncertainty on the refrigerant temperature was assumed to be +0.4 and -0.5°C. The non-symmetrical uncertainty was to ensure that there was not change in the direction of heat transfer between the bulb and refrigerant.

Figure 3.5 shows the effect of the uncertainty on the refrigerant and bulb temperatures. A range of possible bulb time constants could then be found to determine how broad the range might be for the bulb time constant that was measured.

Equation 3.3 was used to find the possible range of values for the bulb time constant within the temperature uncertainty. As measured by the thermocouples, the bulb time constant was approximately 150 to 200 seconds. If the thermocouples were incorrect and the temperature difference between the refrigerant and bulb was actually larger, the bulb time constant could have ranged from 200 to 700 seconds. On the other hand, if the temperature difference between the bulb and refrigerant was smaller than measured, the bulb time constant could have ranged from 0 to 100 seconds. As the refrigerant temperature approaches the bulb temperature, the denominator in Equation 3.3 goes to zero, hence the bulb constant tends toward zero in that case. Figure 3.6 shows the range of bulb constants that could be encountered within the thermocouple uncertainty.

3.3.3 Bulb time constant - analytical solution

Equation 3.1 can be simplified into Equation 3.4 to find the time constants analytically. As shown in Equation 3.3, the time constants can also be determined from the convection coefficients, contact area with the flow, and the bulb mass and specific heat. The time constants for the bulb when responding to both the refrigerant and the air flow were approximately 200 and 900 seconds, respectively.

$$\frac{1}{\tau_r}\left(T_{r,o} - T_b\right) + \frac{1}{\tau_{air}}\left(T_{rm} - T_b\right) = \frac{dT_b}{dt} \tag{3.4}$$

where

$$\tau_r = \frac{M_b c_b}{A_{cont} h_{r,o}} \approx \frac{(0.027\ \text{kg})(385\ \text{J/kgK})}{(0.00018\ \text{m}^2)(300\ \text{W/m}^2\text{K})} \approx 190\ \text{sec}$$

$$\tau_{air} = \frac{M_b c_b}{A_{b,sur} h_{air}} \approx \frac{(0.027\ \text{kg})(385\ \text{J/kgK})}{(0.00146\ \text{m}^2)(8.22\ \text{W/m}^2\text{K})} \approx 890\ \text{sec}$$

3.3.4 Refrigerant-side convection coefficient

While the refrigerant-side convection coefficient is included in the analytical calculation of the bulb time constant, the convection coefficient is not a constant for all flow conditions exiting the evaporator. For example, pure vapor exiting the evaporator will have a lower convection coefficient than if two-phase flow exits the evaporator. Because the refrigerant convection coefficient may change during evaporator transients, the bulb time constant may undergo slight variations as well.

Random fluctuations in the liquid dry-out point occur for up to 10% of the two-phase length [13-14]. It then follows that if the two-phase length is greater than 90% of the evaporator passage, it is possible for liquid drops (two-phase flow) to exit the evaporator and increase the refrigerant-side heat transfer coefficient. To account for the higher convection coefficient of two-phase flow when calculating the bulb time constant, a linear relationship was assumed between the convection coefficient for a pure superheat exit and the convection coefficient for a two-phase exit. This relationship was used in the last ten percent of the evaporator length, as shown in Figure 3.7.

3.4 Spring Characteristics

3.4.1 Spring constant

The spring constant is prescribed as a characteristic of the expansion valve. If the spring constant is not known for a particular valve being modeled, it can still be estimated if other valve design parameters are known along with the operating temperature range of the valve. The range of pressure acting on the diaphragm by the bulb can be calculated from the offset temperature and maximum operating temperature of the valve. The maximum change

in force felt by the spring (ΔF) is found by multiplying the maximum change in pressure by the diaphragm area. Since the overall deflection (δ) of the spring can be found from the pin angle and orifice size, the spring constant can be estimated by Equation 3.5. The representative thermostatic expansion valve used for geometrical measurements had a spring constant of approximately 50 kN/m.

$$k_{sp} = \frac{\Delta F_{sp}}{\delta_{sp}} \tag{3.5}$$

3.4.2 Force on closed valve

The force the spring exerts on a closed valve is determined from the expansion valve design, however, it can be changed by turning a screw that adjusts the spring deflection. The valve behavior can then be changed to produce a different evaporator superheat. If the screw is used to further compress the spring a higher superheat is needed to open the valve and if the screw is used to relax the spring less superheat is needed to open the valve. The spring force acting on a closed valve can be found from Equation 3.6 if the initial spring force, the spring constant, and the screw deflection are known.

$$F_{sp,cl} = F_{sp,initial} + k_{sp}\delta_{screw} \tag{3.6}$$

3.4.3 Spring deflection

The spring deflection needs to be known in order to find the effective orifice area. The force exerted by the spring at any given time can be found from a force balance on the diaphragm, as shown in Equation 3.7. Then, since the spring force is a linear function of the deflection, the deflection of the spring can be found from Equation 3.8.

$$F_{sp} = (P_b - P_{sl})A_{diaph} \tag{3.7}$$

$$\delta_{sp} = \frac{F_{sp} - F_{sp,cl}}{k_{sp}} \tag{3.8}$$

3.5 Mass Flow Rate

3.5.1 Maximum valve flow rate

The maximum flow rate for a given valve is a function of the pressure drop across the valve and the size of the orifice. The flow rate can be increased by either increasing the orifice diameter or the pressure drop across the orifice. The maximum flow rate for a given orifice is calculated by an empirical correlation shown in Equation 3.9, developed by Hrnjak [36].

$$m_{max} = c1 \cdot A \cdot \sqrt{2 \cdot \rho \cdot [P_{in} - P_{sat} \cdot K]} \tag{3.9}$$

where

$$K = c2\left(\frac{S+2}{T_c}\right)^{c3} + d^{c4}L^{c5} + c6 + c7\left(\frac{P_c - P_{out}}{P_c}\right)$$

and

$c1 = 2.6525(10^{-1})$ $c2 = -1.1497(10^{-1})$ $c3 = 4.1466(10^{-2})$

$c4 = -6.5783(10^{-3})$ $c5 = 3.9001(10^{-3})$ $c6 = 2.1867(10^{-5})$

$c7 = 3.6292(10^{-2})$

m_{max} = max flow rate through valve [g/sec] ρ = liquid density [kg/m^3]

A = area of valve opening [mm^2] S = subcooling [°C]

P_{in} = inlet pressure [bar] d = hole diameter [mm]

P_{sat} = saturation pressure [bar] L = passage length [mm]

P_c = critical pressure [bar] T_c = critical temperature [K]

P_{out} = evaporator pressure [bar]

Because of the magnitude of the pressure drop across the orifice, small perturbations of the evaporator pressure do not have a large influence on the flow rate through the valve. However, because the condenser pressure is high, small percentage-wise fluctuations in the condenser pressure may cause significant changes in the flow rate.

3.5.2 Actual flow rate

The actual mass flow rate into the evaporator is calculated by assuming refrigerant flows through a circular orifice that is partially obstructed by a conical pin moving up or down. A close-up view of the flow passage obstructed by the pin is shown in Figure 3.8. If the pin deflection is zero no refrigerant flows through the orifice, and if the pin deflection is at some maximum value the pin will not obstruct the flow and the valve will be operating at the maximum flow rate. The effective orifice area is calculated by subtracting the obstructing area of the pin from the area of the valve orifice, as shown in Figure 3.9. The actual flow rate through the valve can then be calculated from Equation 3.10.

$$m_{TXV} = \left(\frac{A_{orif} - A_{pin}}{A_{orif}} \right) m_{max} \tag{3.10}$$

3.6 Offset Temperatures

Changing the valve design parameters, such as the spring constant, initial spring force, and maximum pin deflection, will change the range of operating superheat shown in Figure 3.2. To find the offset temperature of a given valve, a force balance on the diaphragm is first used to find the pressure exerted by the bulb to just open the valve, as seen in Equation 3.11. Because the fluid inside the bulb is two-phase, this bulb pressure found from Equation 3.11 corresponds to the temperature of the bulb, T_{cl}, when the valve just opens from a closed position. The saturation temperature of the exit refrigerant can be subtracted from the saturation temperature of the bulb fluid to find the offset temperature needed to open the valve, as shown in Equation 3.12.

$$P_{b,cl} = \frac{F_{sp,cl}}{A_{diaph}} + P_{sl} \tag{3.11}$$

$$T_{offset} = T_{cl} - T_{r,i} \tag{3.12}$$

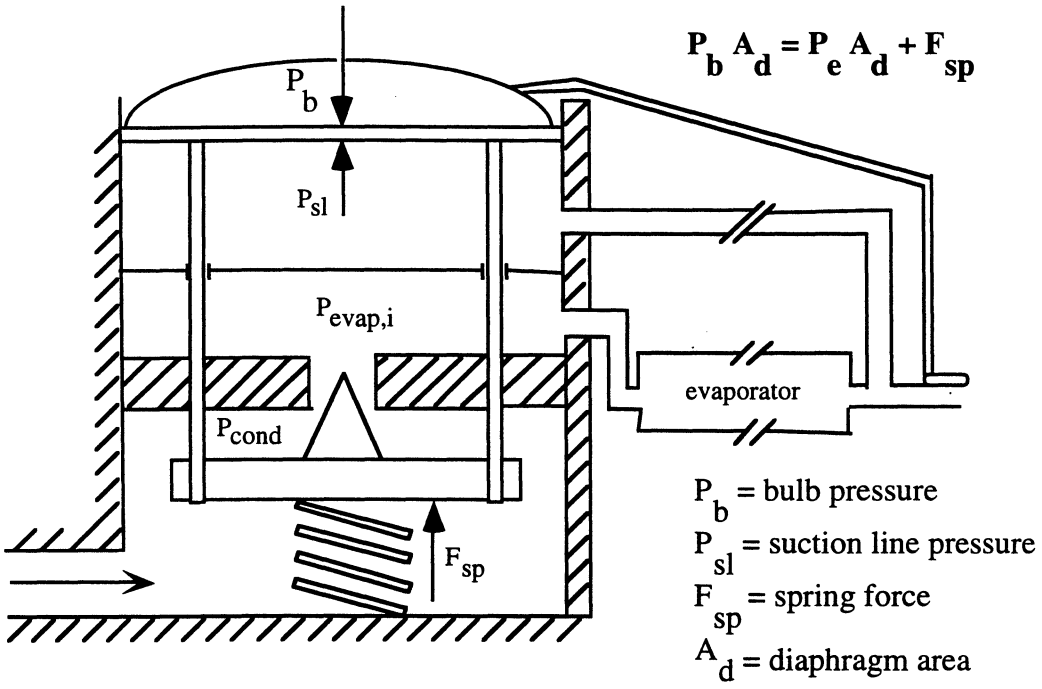

Figure 3.1 Diagram of a thermostatic expansion valve. The bulb and suction-line pressure act on the diaphragm and, coupled with the spring force, control the effective orifice area. The evaporator inlet and condenser pressure influence the flow rate through the orifice.

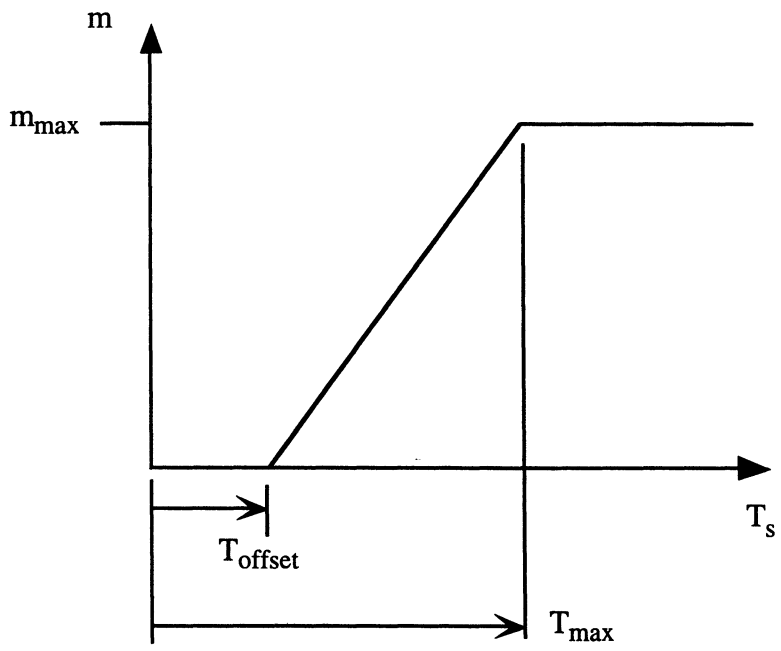

Figure 3.2 Simplified flow rate vs. superheat curve showing the relationship between offset temperature, maximum superheat, and mass flow rate through the expansion valve.

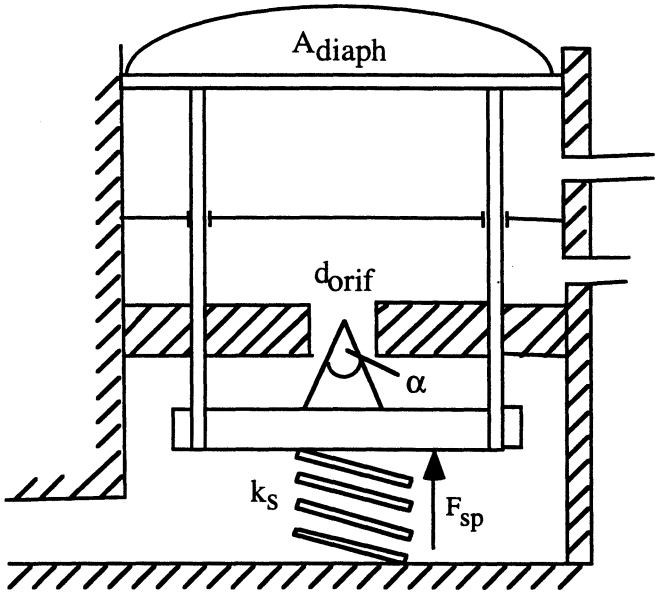

Figure 3.3 Expansion valve design parameters: diaphragm area, A_{diaph}, orifice diameter, d_{orif}, pin tip angle, α, spring constant, k_s, spring force on a closed valve, F_{sp}, and bulb constant (not shown), τ_b.

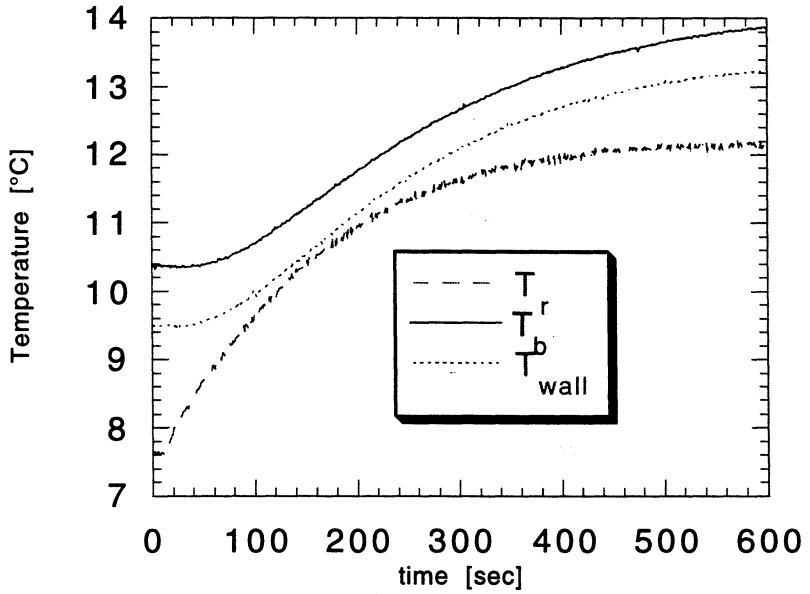

Figure 3.4 Experimental results of a refrigerant temperature increase and the corresponding suction line wall and valve bulb temperature increase.

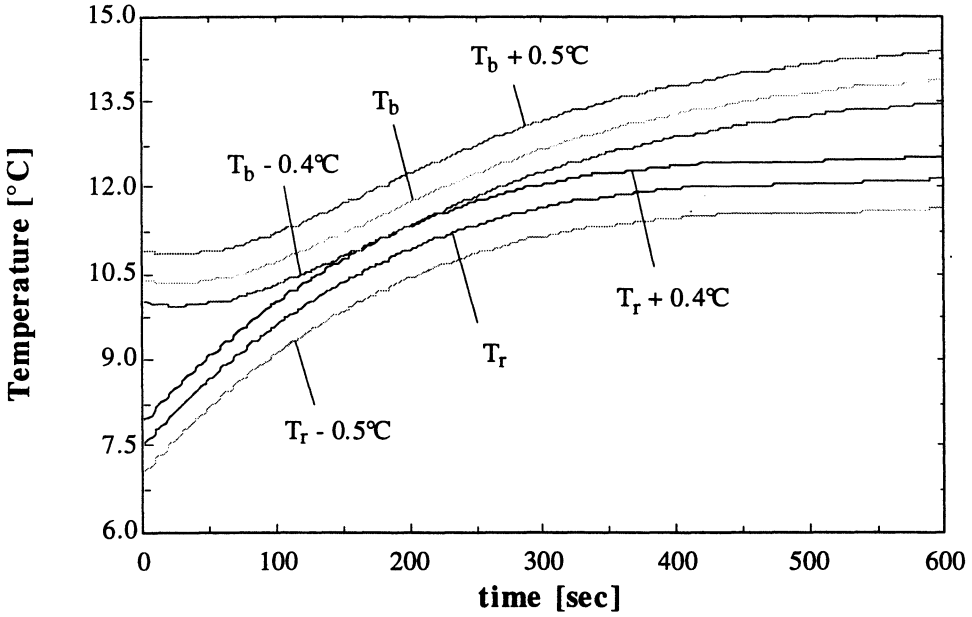

Figure 3.5 Bulb and refrigerant temperature measurements and their uncertainty. Bulb temperature was assumed to be +0.5/-0.4°C, and refrigerant temperature was assumed to be +0.4/-0.5°C.

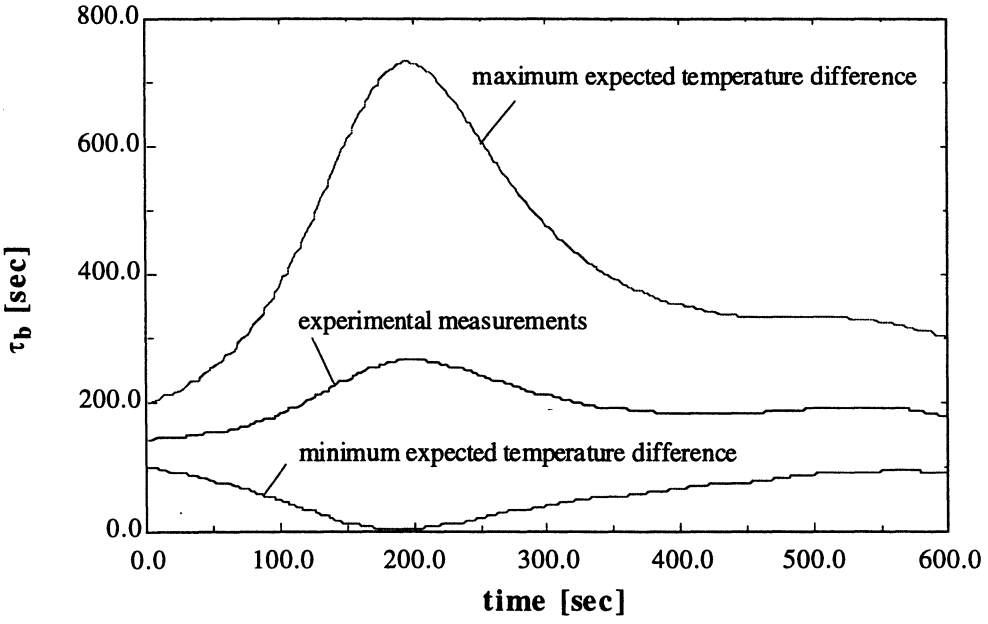

Figure 3.6 Bulb time constant as measured by the thermocouples, and the time constant variation expected by the maximum thermocouple uncertainty.

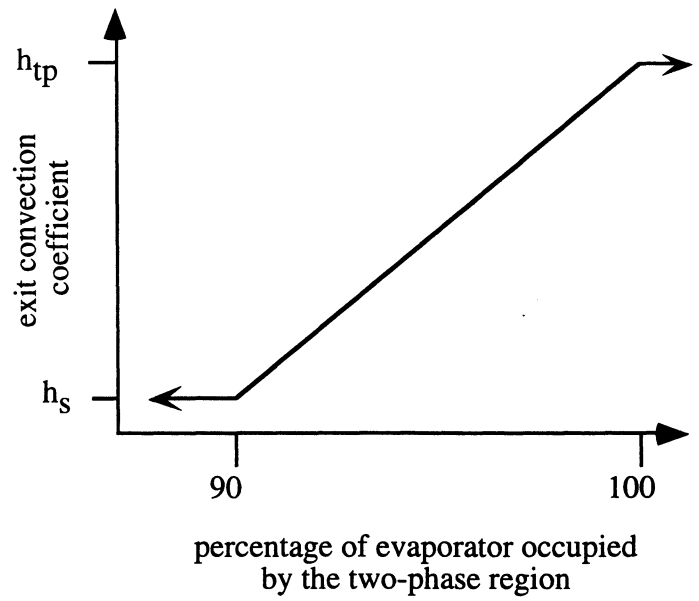

Figure 3.7 Variation of the refrigerant-side convection coefficient near the exit of the evaporator. A linear relationship is assumed between the convection coefficient for superheated vapor and two-phase flow in the last 10% of the evaporator passage.

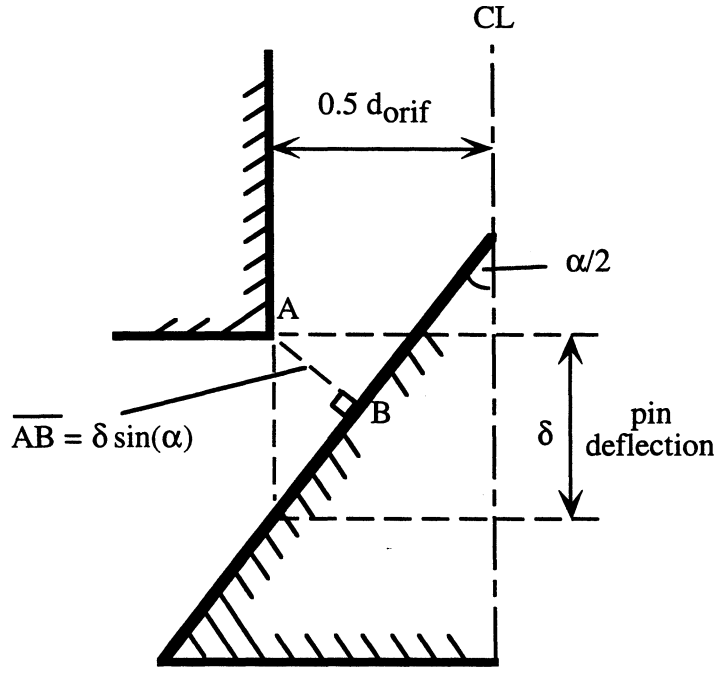

Figure 3.8 Cross-section of the expansion valve orifice and obstructing pin. The effective flow area is shown by the line AB, which is a function of the pin deflection, δ, and pin tip angle, α.

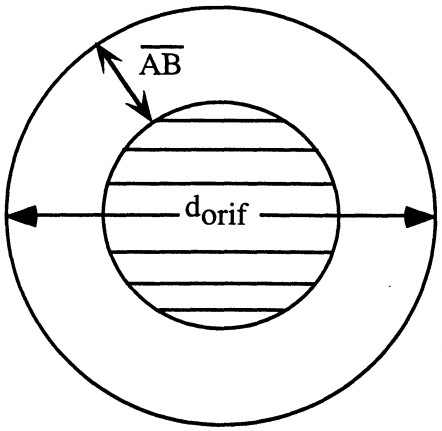

Figure 3.9 Approximation of the effective orifice area seen by the refrigerant, where line AB is shown in Figure 3.8. The pin obstruction is shown by the inner circle. Refrigerant flows through the annulus created by the pin.

CHAPTER 4 - RESULTS AND DISCUSSION

4.1 Introduction

It is well known that steady-state conditions do not truly exist in an evaporating system. Random fluctuations in the two-phase length, thermal non-equilibrium at the evaporator exit, and slug propagation through the evaporator all lead to fluctuating conditions within the flow. Therefore, drawing a line between what constitutes a stable system or an unstable system is difficult; however, a system definitely crosses the line into unacceptable behavior when the efficiency is reduced or components may become damaged or undergo excessive wear due to the transients.

Hunting has been defined as "a condition that occurs when a controller [...] continuously overrides and undershoots or overshoots the control point, with resulting fluctuation and loss of control of the condition to be maintained [37]." The control condition to be maintained with a thermostatic expansion valve is the superheat signal. Thermostatic expansion valves may hunt under nearly uniform air-side evaporator conditions, implying there must be a mechanism internal to the evaporator loop triggering these oscillations, possibly due to the stochastic nature of the two-phase flow or the effects of the compressor. While the modeling methods described in Chapters 2 and 3 average out the effects of thermal non-equilibrium and slug flow, in a real system they do occur, and one effect they have is on the suction-line pressure.

Barnhart [17] have shown that slug formation in the evaporator leads to suction-line pressure oscillations at the exit, even for what would be considered steady operation. These pressure oscillations induced flow rate oscillations of up to 0.5% through a fixed-size orifice. However, similar to Mumma's investigation [14], the refrigerant exit temperature remained constant. Nonetheless, even with a constant refrigerant exit temperature, Barnhart saw an oscillating superheat because the saturation temperature was changing. A

thermostatic expansion valve could magnify these disturbances in flow rate and superheat for two reasons. First, the suction-line pressure oscillations act on the valve diaphragm to move the pin setting, and second, a thermostatic expansion valve would react to the fluctuating superheat reading.

4.2 Application of Model

Any cyclic perturbation in the evaporating system will cause a disturbance to propagate through the system. This disturbance may die out by the time it reaches the evaporator exit, or it may become magnified and show up as large changes in the exit superheat. These cyclic perturbations may be small changes in the water-side flow rate, refrigerant flow rate, liquid-line pressure, or the suction-line pressure, just to name a few. A sinusoidal suction-line pressure was chosen to represent these various disturbances in the system, and the effect on the evaporator superheat was examined by using the model of the evaporator and thermostatic expansion valve that was developed. It is realized that the quantitative results may differ for the different perturbation elements, but the general system response is expected to be the same whether oscillating the suction-line pressure or, say, the condenser pressure. The effect of a sinusoidal suction-line pressure was analyzed at various frequencies, along with the effect of different thermostatic expansion valve designs—varying the bulb time constant, orifice diameter, pin tip angle, spring constant, diaphragm diameter, and initial spring force.

The suction-line pressure was prescribed to be 315 kPa +/- 1%, corresponding to a range of saturation temperatures from 1.73°C to 2.30°C. The peak-to-peak amplitude of the superheat response was then plotted versus the suction-line frequency; the peak-to-peak amplitude being the difference between the maximum and minimum superheat during the oscillation. For example, Figure 4.1 shows the superheat response to reach regular oscillations between 3.4°C and 5.9°C, a range of 2.5°C, when the suction-line pressure oscillated at 1/80 Hz.

The effect of a step change in suction-line pressure was also examined using the model. The transients following a single perturbation will vary in size and duration, depending on the expansion valve design. Therefore, the time-domain response shows how the valve parameters influence the steady-state superheat as well as the rate at which the perturbation is damped out before reaching new steady-state conditions.

The system response to a single perturbation was examined by allowing the evaporator and valve to reach steady-state and then increasing the suction-line pressure over a period of ten seconds. The suction-line pressure was increased from 315 kPa to 324 kPa, corresponding to a refrigerant saturation temperature increase from 2.0°C to 2.8°C. A physical condition that may initiate a sudden change in the suction-line pressure might be a change in the compressor speed.

A sudden increase in the suction-line pressure affects the expansion valve by increasing the force on the bottom side of the diaphragm, further closing the valve and decreasing the flow rate, as shown in Figure 4.2. As the flow rate drops, the superheat will increase and warm the bulb at the evaporator exit. After the step increase in pressure, the bulb pressure via the superheat is the sole influence regulating the flow rate through the expansion valve. The design of the expansion valve can be better understood by isolating certain components in the valve and examining their effect on evaporator transients.

4.3 Valve Parameters

The expansion valve parameters that were examined were the bulb time constant, orifice diameter, pin tip angle, spring constant, diaphragm diameter, and the spring force on a closed valve. One parameter was varied while all others were held constant in order to see the effect of that one parameter. Therefore, no constraints were imposed to keep the steady-state superheat a constant—it was allowed to vary. The effect of each of these parameters is shown in Figures 4.3 through 4.14.

4.3.1 Bulb time constant

The expansion valve bulb attached to the exit of the evaporator is used to sense and control the evaporator superheat. If the bulb temperature rises in response to the evaporator exit conditions, the valve will open further and allow an increased refrigerant flow rate. On the other hand, if the bulb temperature decreases the valve will respond by closing and restricting the flow rate. If the bulb temperature ever drops below the offset temperature of the valve, the valve will close and no refrigerant will enter the evaporator.

The rate at which the bulb responds to changing evaporator exit conditions is a function of the bulb mass, specific heat, and contact area with the evaporator. A large bulb with a high thermal resistance will not experience rapid temperature changes and the bulb will take longer to respond to a change in the system. On the other hand, a small bulb or one with less thermal resistance will respond more quickly to changing evaporator exit conditions and will be more influential in regulating the superheat.

Figure 4.3 shows how the bulb time constant affects the magnitude of the superheat fluctuations during a suction-line pressure oscillation. The time constants used for the analysis ranged from 10 to 70 seconds, a range expected for the fastest responding bulbs. A valve with a lower bulb time constant is shown to better control the superheat fluctuations, as it can quickly adjust the flow rate to control the superheat. On the other hand, the valve with a large bulb constant reacts more slowly to the changing superheat and the oscillations nearly triple in magnitude from that of the larger constant.

Figure 4.4 shows how the bulb time constant influences valve behavior for a step increase in suction-line pressure. The superheat initially decreases following a step increase in the suction-line pressure due to the rising saturation temperature. Following the quick drop in flow rate, the superheat begins to rise and the bulb with the lowest time constant is able to respond the fastest, minimizing the superheat fluctuations that follow.

4.3.2 Orifice diameter

An important part of expansion valve design is the size of the orifice through which the refrigerant flows. As the capacity of the evaporator increases, so should the size of the orifice in order to allow for higher refrigerant flow rates. Care should be taken not to include an oversized valve for the application though, as an oversized valve will operate in a nearly closed position for the flow rate to be kept low enough to ensure adequate superheat.

The effect of the orifice diameter when responding to pressure oscillations can be seen in Figure 4.5, where small changes in orifice size have a large impact on the superheat response. A large orifice area makes the valve less stable, as larger flow rate oscillations are possible which lead to large changes in superheat. Decreasing the orifice area decreases the superheat fluctuations by decreasing the change in flow rate for a given change in superheat. Figure 4.15 shows the effect of orifice sizes by comparing two flow rate-versus-superheat curves for a given condenser and suction-line pressure. Each curve has the same offset temperature and maximum superheat, but they differ in the fact that curve "A" has a greater maximum flow rate due to a larger orifice diameter. Decreasing the orifice area would then shift the curve from "A" to "B". The slope of the flow rate versus superheat curve is smaller for "B", resulting in smaller changes in flow rate for a given change in superheat.

Figure 4.6 shows how valves with different orifice sizes have different steady-state operating points and how the superheat response differs following a step change in suction-line pressure. For the given pressure drop across the valve, the maximum flow rates for the orifice diameters of 0.6, 0.7, and 0.9 mm are approximately 4.6, 6.3, and 10.5 g/sec, respectively. Under the imposed water-side heat transfer conditions, the evaporator could fully evaporate the refrigerant with an inlet flow rate of approximately 2.5 g/sec; the above orifice sizes were chosen that would allow significantly higher flow rates.

A difference in the steady-state superheat of more than 1°C separates the large and small valve. Because the larger valve is capable of handling a higher flow rate, the exit superheat needs to be lower to keep the valve in a more closed position. Following a step change in operating conditions, the larger valve also has superheat fluctuations that are larger and have a higher frequency. While the initial pressure disturbance will deflect the valve pin equally in all cases (all other conditions being equal), the valve with the larger orifice will experience a greater change in flow area, thus allowing more refrigerant into the evaporator and larger changes in superheat.

4.3.3 Pin tip angle

The angle of the pin tip is sometimes used to control the behavior of an expansion valve. A pin with a large tip angle is relatively flat and therefore the flow is sensitive to small changes in deflection. On the other hand, the flow is less sensitive to changes in deflection with a small pin tip angle because the change in flow area is not as great for a given deflection.

The effect of the pin tip angle on superheat oscillations resulting from pressure oscillations can be seen in Figure 4.7. Valves with a large pin angle experience large changes in superheat, while a small pin angle keeps the superheat oscillations minimal at all suction-line pressure oscillation frequencies. The pressure oscillations deflect each pin equally, but the change in flow rate is much less for a small angle pin. The stabilizing effect of decreasing the pin tip angle can be explained through the flow rate versus superheat curves shown in Figure 4.16. Two curves are shown depicting different valves with the same offset temperature and maximum flow rate, but the valves need to reach different levels of superheat before they are fully open. Decreasing the pin tip angle increases the maximum superheat needed to open the valve because a greater bulb pressure is needed to push the longer pin out of the orifice. Thus, using a smaller angle pin moves the curve

from "A" towards "B", where a given change in superheat will produce a smaller change in flow rate.

Figure 4.7 shows how the pin tip angle affects the superheat response to a sudden suction-line pressure increase. As with different orifice sizes, the steady-state superheat values are significantly different when the pin tip angle is changed. Because a pin with a large tip angle needs to deflect less to produce the needed flow rate (from the closed position), less superheat is needed at steady state. The pressure perturbation will also have a greater effect on the valve superheat when a large pin tip angle is used because it experiences larger changes in flow rate for the same deflection. On the other hand, the valve with a small pin tip angle hardly registers a response when the suction-line pressure changes because there is little change in the effective flow area through the orifice.

4.3.4 Spring constant

The expansion valve spring applies the extra force needed to balance the pressure difference between the bulb and the suction line. Changing the spring constant affects the rate at which the valve opens for a given change in bulb temperature; a higher spring constant allows the pin to deflect less to balance the forces on the diaphragm. The spring constant also helps determine the operating temperature range of the expansion valve, and it is usually chosen to allow for a 10-15°C temperature range from a closed valve to the maximum flow rate.

Figure 4.9 shows that valves using a smaller spring constant experience greater superheat fluctuations than valves with a larger spring constant. The spring constants were chosen to allow for a 12°C, 14°C, and 16°C superheat operating range for the valve. A stiff spring increases the force needed to deflect the pin a given distance, meaning that a greater change in superheat is needed to change the flow rate a given amount. The flow rate versus superheat curve shown in Figure 4.16 again shows the effect of changing the spring constant, where increasing the spring constant increases the superheat needed to reach the

maximum flow rate. Therefore, increasing the spring constant shifts the curve in Figure 4.16 from "A" to "B", stabilizing the valve.

Figure 4.10 shows the superheat response for different spring constants following a step change in suction-line pressure. The difference in the steady-state superheat is because a small spring constant forces the pin to deflect more to balance the forces on the diaphragm. The greater pin deflection allows a higher refrigerant flow rate through the valve, which decreases the superheat. The effect of the spring constant on superheat transients can also be seen, where a small spring constant allows the pin to deflect further for a given change in superheat, increasing the magnitude of the flow rate and superheat oscillations.

4.3.5 Diaphragm diameter

While not usually a candidate for change during valve re-design, the diaphragm does have an effect on the superheat signal. As previously stated, the pressure from the bulb and the suction line act on the diaphragm and are balanced by the spring force. Increasing the size of the diaphragm increases the force difference between the bulb and suction line—making the spring and pin deflect more. On the other hand, a smaller diaphragm will reduce the difference in force from the two pressures, and the spring needs to provide less force for a given difference in diaphragm pressures.

Figure 4.11 shows how a valve with a large diaphragm area increases the magnitude of the superheat oscillations for an unsteady suction-line pressure. What begins as small superheat fluctuations may induce large changes in flow rate, and the change in superheat signal grows even larger. Because the force needed to fully deflect a pin out of the orifice is constant, decreasing the diaphragm area will require a larger superheat to fully remove the pin from the orifice. The effect is again explained through Figure 4.16, where using a smaller diaphragm will shift the valve the curve from "A" to "B" and stabilize the system.

Figure 4.12 shows the superheat response is different for different diaphragm diameters. First of all, the initial steady-state superheat is smaller for a valve with a greater diaphragm area. The smaller superheat comes about because the spring needs to deflect more to balance the force difference on the diaphragm. The transient response shows that a large diaphragm area also makes the valve more sensitive to bulb and suction-line pressure fluctuations. The initial superheat response with the large diaphragm is nearly three times as large as the response with the small diaphragm.

4.3.6 Initial spring force

The spring force exerted on the closed valve is a parameter than can be changed during operation, usually by adjusting a screw in the valve. Turning the screw will increase or decrease the deflection of the spring causing the force to change, thereby affecting the offset temperature.

Figure 4.13 shows that changing the initial spring force does not significantly affect the superheat response during suction-line pressure oscillations at various frequencies. The reason very little effect is seen on the frequency response is because changing the initial spring force does not change the shape of the flow rate versus superheat curve for the valve. Increasing the spring force shifts both the offset temperature and the maximum superheat to the right, keeping the slope the same.

The initial spring force does affect valve performance though, as seen by the response in the time domain shown in Figure 4.14. When the flow rate versus superheat curve is shifted to the right, a higher superheat is required to produce the flow rate needed by the evaporator. Thus, the steady-state superheat largely depends on the spring force. The transient response to a step change in suction-line pressure shows the same thing as Figure 4.13—the magnitude of the superheat oscillations is independent of the initial spring force. Spring forces of 6.0 N, 11.0 N, and 16.0 N were chosen to vary the offset

temperature from approximately 1.5°C to 4.0°C, shown with the steady-state superheat response in Table 4.1.

Table 4.1 The effect of the spring force on offset temperature and refrigerant superheat. The valve will remain closed any time the bulb superheat is less than the offset temperature.

Force [N]	offset temperature [°C]	superheat [°C]
6.0	1.51	4.40
11.0	2.73	5.44
16.0	3.90	6.44

4.4 Valve parameter influence at various perturbation frequencies

The frequency response plots generated for each valve parameter listed above are useful not only in understanding how superheat is affected, but also in understanding *when* certain parameters affect the superheat signal. The valve flow rate, and hence superheat, is mainly controlled by the interaction of the bulb and suction-line pressure on the diaphragm. The rate at which each pressure changes relative to the other will determine what parts of the valve can be used to stabilize the superheat signal.

The frequency response plots (Figures 4.3, 4.5, 4.7, 4.9, 4.11, and 4.13) can each be broken up into three regions, what will hereafter be called the low, middle, and high frequency oscillations. The low frequency suction-line pressure oscillations are on the order of 0.01 Hz or less, where the superheat response is very small. Likewise, the high frequency oscillations, greater than 0.05 Hz, also produce a very small superheat response. Suction-line pressure oscillations in the middle frequency, however, may induce substantial oscillations in evaporator superheat.

The high frequency oscillations, greater than 0.05 Hz, have very little effect on the superheat response. The small changes in the superheat signal are mostly due to the changing saturation temperature of the refrigerant (0.57°C), as opposed to exit temperature oscillations. Therefore, events that may cause a rapidly fluctuating evaporator pressure,

such as the compressor (>10 Hz) or periodic slug flow found by Barnhart (0.33 Hz), do not appear to be a major cause of superheat instability in the evaporator. While these rapid pressure fluctuations may have a significant effect on the flow rate through the valve, the effects of a changing flow rate are mostly damped out by the volume of the evaporator before the disturbance reaches the exit.

Even though the superheat fluctuations are small in the high frequency region, differences in the valve design do have an effect on the magnitude of the superheat oscillation. The important parameters that affect the superheat response in the high frequency region are the orifice diameter (Figure 4.5), pin tip angle (Figure 4.7), spring constant (Figure 4.9), and diaphragm diameter (Figure 4.11). Each one of those plots show that the magnitude of the superheat oscillations can be controlled by the internal valve design, mainly by modifying the flow rate versus superheat curves described in Figures 4.15 and 4.16. On the other hand, the bulb time constant has no influence on the magnitude of the superheat fluctuations for any frequency greater than 0.025 Hz (Figure 4.3). Superheat response is independent of the bulb because of its large thermal mass, making it unable to quickly respond to superheat changes. Therefore, the expansion valve flow control and evaporator superheat is governed solely by fluctuations in the suction-line pressure and the internal geometry of the valve. Feedback of the superheat signal does not sustain the valve hunting.

If the suction-line pressure oscillates in the low frequency range, less than 0.01 Hz, the superheat response is again somewhat small. The gradual changes in flow rate induced by a changing suction-line pressure act over such a long time that the expansion valve bulb has a chance to sense the changes in superheat and correct for the change in flow rate. At low frequencies, the bulb pressure response is significantly faster than the suction-line pressure changes.

In the low frequency range, the bulb time constant now plays a role in the magnitude of the superheat response (Figure 4.3). A large time constant does not allow the

bulb to sense the changes in superheat as fast as a small time constant would, so control of the flow rate is not very well maintained. Unlike the region of high frequency oscillations, the frequency response plots show that the internal characteristics of the valve such as the orifice size, pin tip angle, spring constant, and diaphragm diameter, lose their significance and do not affect the superheat; the superheat fluctuations are independent of these parameter changes. In these low frequency perturbations, superheat is then controlled solely by temperature feedback mechanisms and is independent of the internal geometry of the valve.

Suction-line pressure oscillations in the middle range of frequencies can produce large changes in superheat. The evaporator cannot damp out the changes in flow rate produced by the suction-line pressure, and the bulb cannot respond fast enough to compensate for the pressure imbalance on the diaphragm. For the given evaporator geometry, the critical period of these oscillations where the superheat signal undergoes large changes (greater than 1°C) is on the order of 40 to 120 seconds. This is not unrealistic, as hunting periods have been seen to range on the order of 30 seconds [10], 100 seconds [12], 120 seconds [15], and 135 seconds [5] in experimental investigations.

The question that might be raised concerns what the underlying cause might be for some perturbation to act at in this frequency range, when the effects of the compressor and slug initiation have already been discounted as being too fast. One possible explanation for periodic behavior in this dangerous middle frequency band might be the occurrence of liquid droplets exiting the evaporator. While it has already been mentioned that Barnhart found that slug instabilities were very periodic with a frequency of 0.33 Hz, he also took measurements of the entrained mass fraction (EMF) at the evaporator exit, a measurement of droplets exiting the evaporator resulting from slugs coalescing into one big slug. His results show that, over an 800 second sample time, there were ten periods where the liquid mass at the exit approached one percent of the total flow. While the distribution in time was erratic, it is interesting to note that he found liquid exiting the evaporator on average every

60 seconds. The effect of these liquid slugs on a thermostatic expansion valve would be two-fold: first there would be a rapid decrease in the exit superheat and, second, the suction-line pressure would be adjusted as the compressor takes in a higher mass flow rate due to the higher density of the liquid. The effect of liquid exiting the evaporator may have a significant impact on the suction-line pressure, enough to generate feedback at frequencies shown to induce large fluctuations in the superheat.

In conclusion, if the suction-line pressure fluctuations are much faster than the bulb pressure fluctuations, the valve behavior will be controlled by the parameters on the bottom (suction-line pressure) side of the diaphragm. For example, if hunting is occurring at high frequencies, changing the response time of the expansion valve will do nothing to correct the problem. On the other hand, when the bulb pressure is able to respond faster than the suction-line pressure, the valve is controlled by the superheat feedback from the bulb. In this case, when hunting at low frequencies, changing the valve capacity or pin tip angle will not affect the superheat signal.

4.5 Suction-line perturbation amplitude

While the frequency response plots showed how the suction-line pressure affected superheat at a given frequency, the effect of the perturbation amplitude is not seen. To understand what the effect of the perturbation amplitude is on the superheat, the superheat response was analyzed for different amplitude perturbations at a frequency of 0.0125 Hz, near where some of the superheat peaks were shown to occur. As can be expected, Figure 4.17 shows that the superheat oscillations grow as the suction-line pressure oscillation amplitude grows; and in the region between a zero and 1.5% perturbation (corresponding to a saturation temperature ranges from 1.45°C to 2.57°C), the growth is linear. For larger suction-line pressure oscillations, the superheat response is less than what would be predicted with a linear relationship with perturbation amplitude due to the fact that the exit convection coefficient increases as the superheat decreases. The curve in Figure 4.17 will

eventually level off to a value set by the difference between the inlet water temperature and the refrigerant saturation temperature as the perturbation amplitude grows.

Dividing the magnitude of the superheat fluctuations by the maximum possible fluctuation would show the size of the oscillations relative to how large the oscillations could potentially be. Therefore, the information in Figure 4.17 can be normalized by the maximum possible oscillation, with the result shown in Figure 4.18. Because the relationship between superheat and perturbation amplitude is linear for small suction-line disturbances, the frequency response plots can be developed once per application and then easily adjusted to fit the perturbation magnitude.

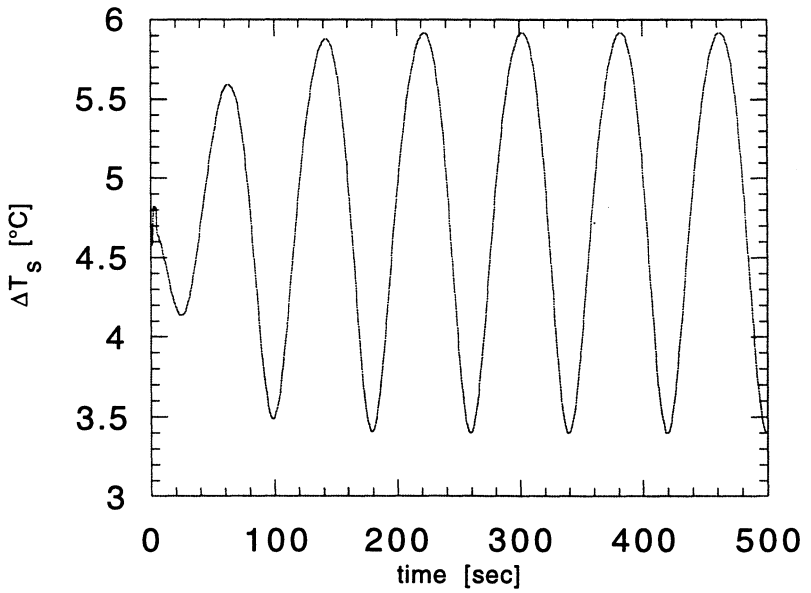

Figure 4.1 Superheat response for a sinusoidal suction-line pressure with a period of 80 seconds. The peak-to-peak amplitude of the superheat is $\Delta T_{s,pp} = 2.5°C$.

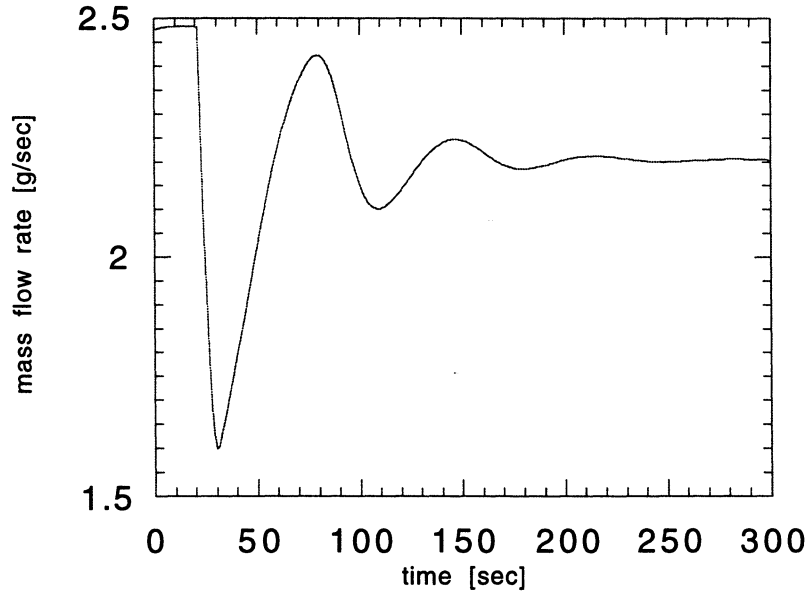

Figure 4.2 Mass flow rate through the expansion valve following suction-line pressure increase from 315 kPa to 324 kPa.

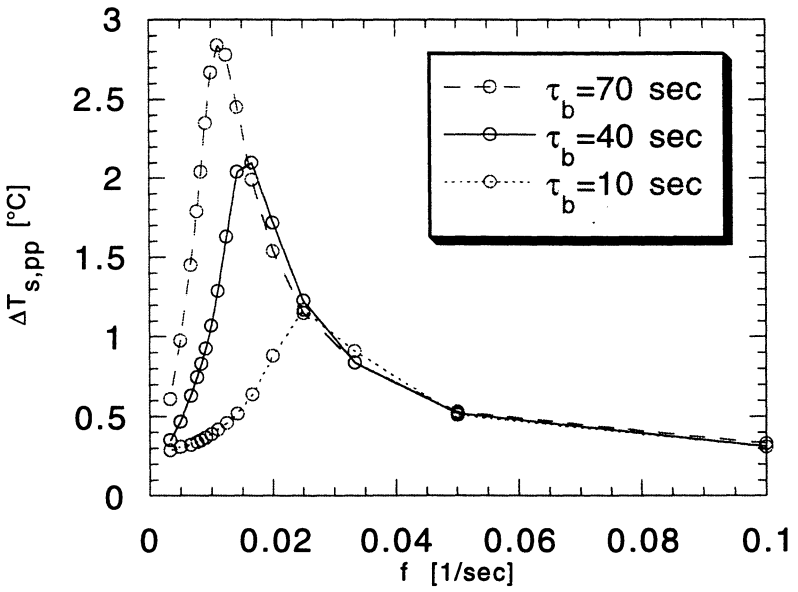

Figure 4.3 Peak-to-peak superheat response for different bulb time constants. Suction-line pressure is 315 kPa +/- 1%, perturbed at different frequencies.

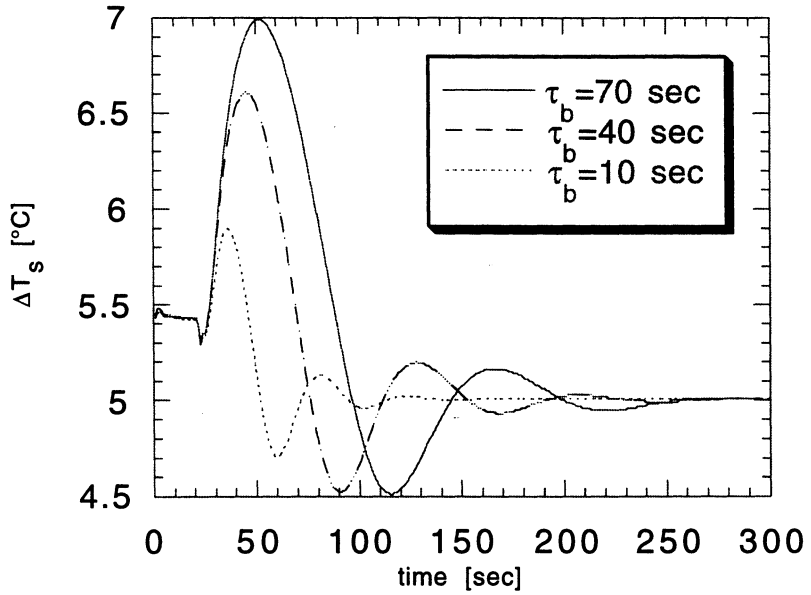

Figure 4.4 Superheat response for different bulb time constants following a step increase in suction-line pressure from 315 kPa to 324 kPa.

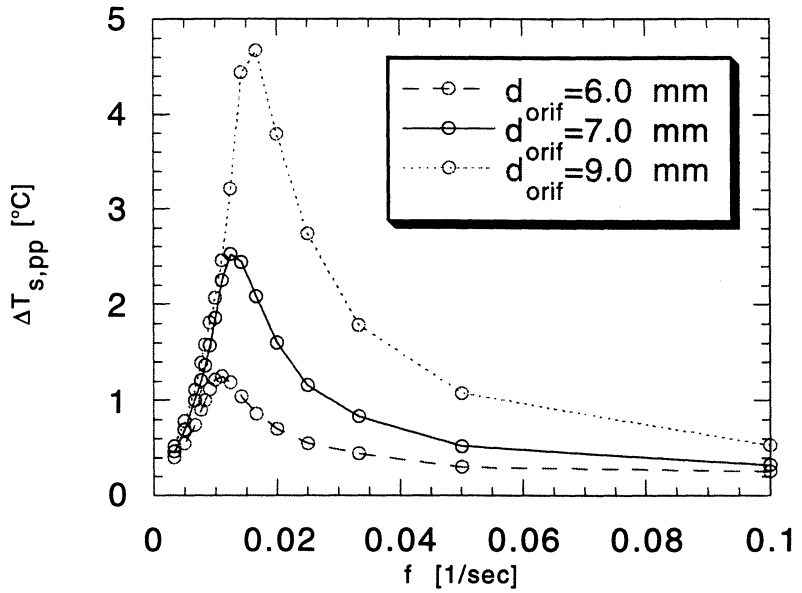

Figure 4.5 Peak-to-peak superheat response for different orifice diameters. Suction-line pressure is 315 kPa +/- 1%, perturbed at different frequencies.

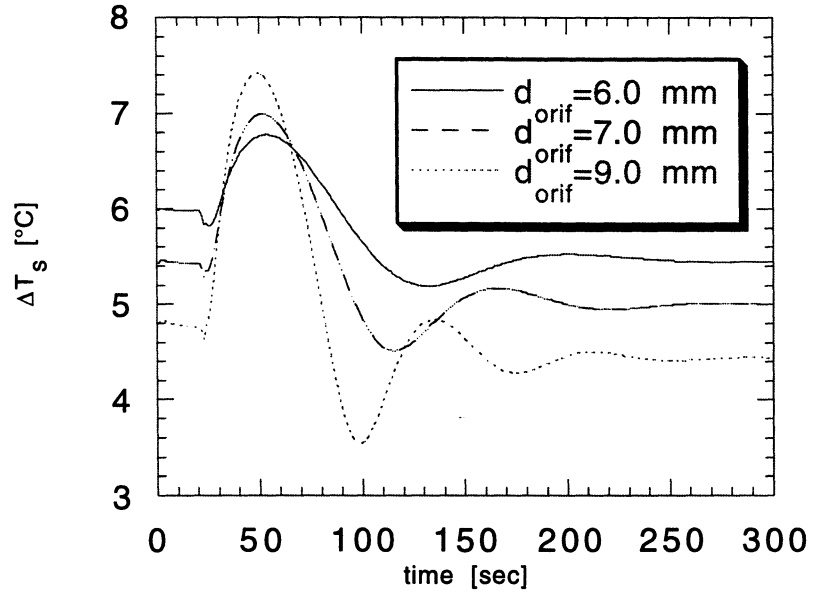

Figure 4.6 Superheat response for different orifice diameters following a step increase in suction-line pressure from 315 kPa to 324 kPa.

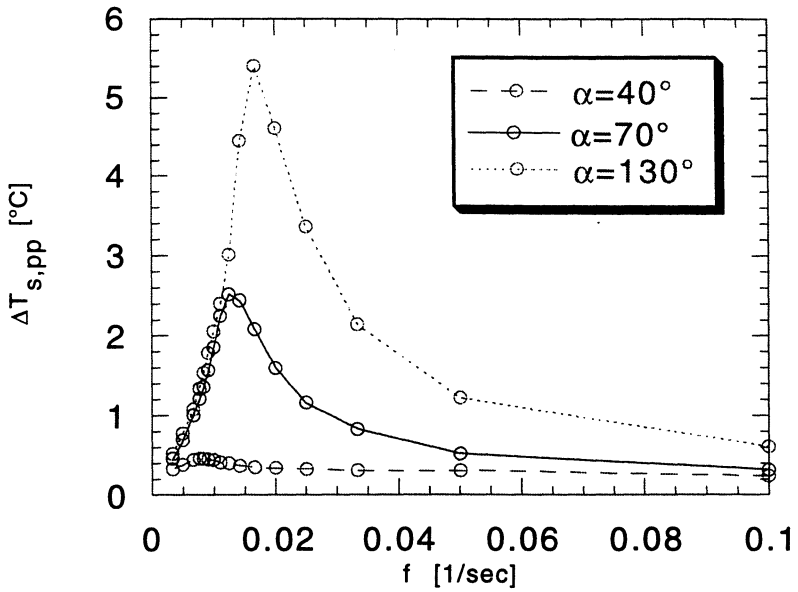

Figure 4.7 Peak-to-peak superheat response for different pin tip angles. Suction-line pressure is 315 kPa +/- 1%, perturbed at different frequencies.

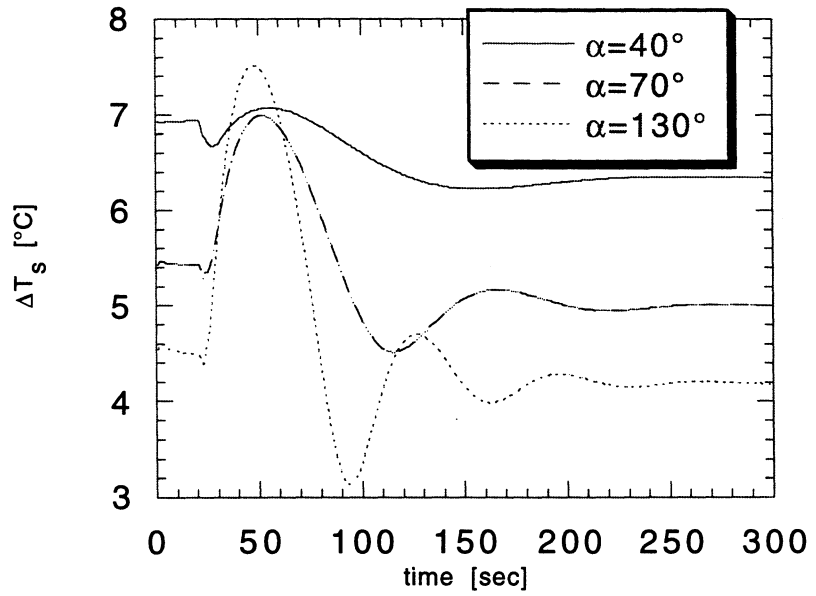

Figure 4.8 Superheat response for different pin tip angles following a step increase in suction-line pressure from 315 kPa to 324 kPa.

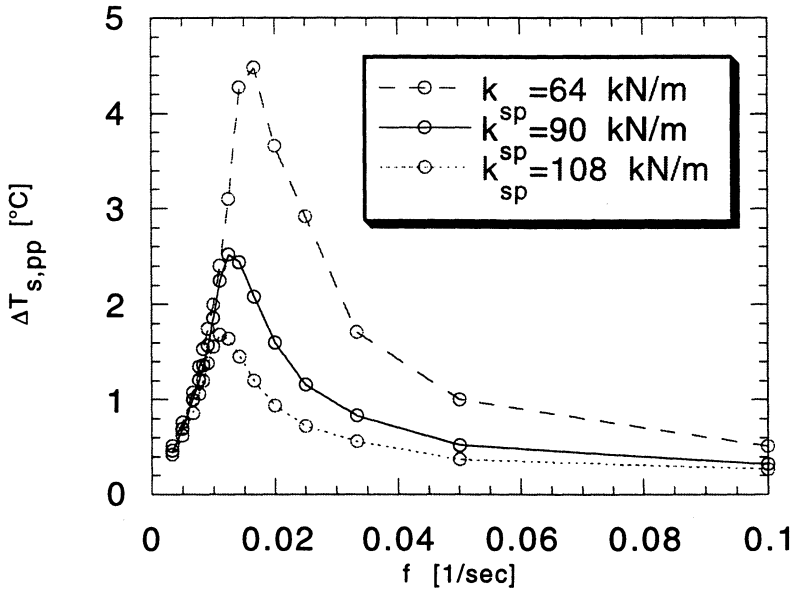

Figure 4.9 Peak-to-peak superheat response for different spring constants. Suction-line pressure is 315 kPa +/- 1%, perturbed at different frequencies.

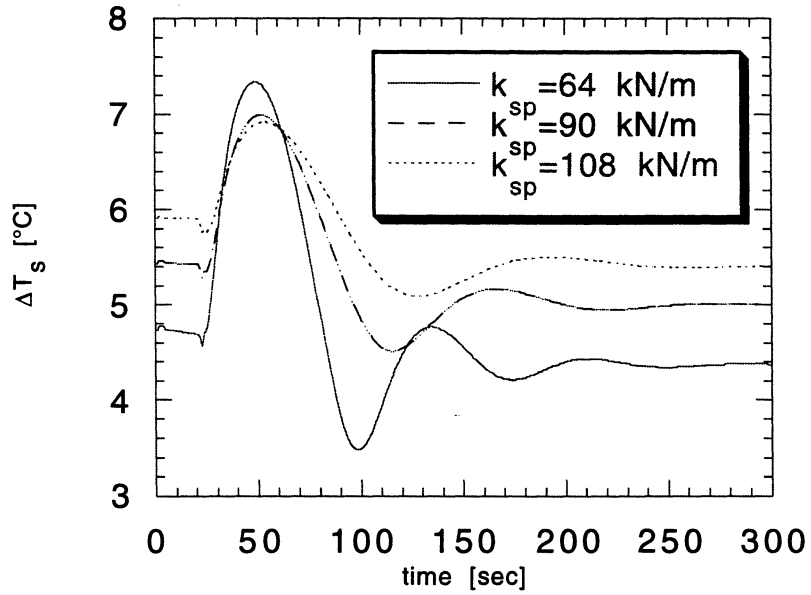

Figure 4.10 Superheat response for different spring constants following a step increase in suction-line pressure from 315 kPa to 324 kPa.

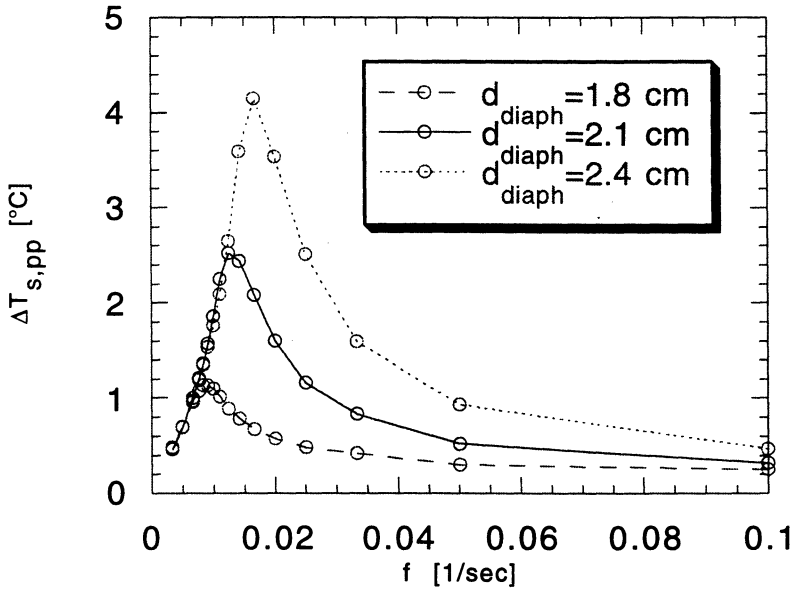

Figure 4.11 Peak-to-peak superheat response for different diaphragm diameters. Suction-line pressure is 315 kPa +/- 1%, perturbed at different frequencies.

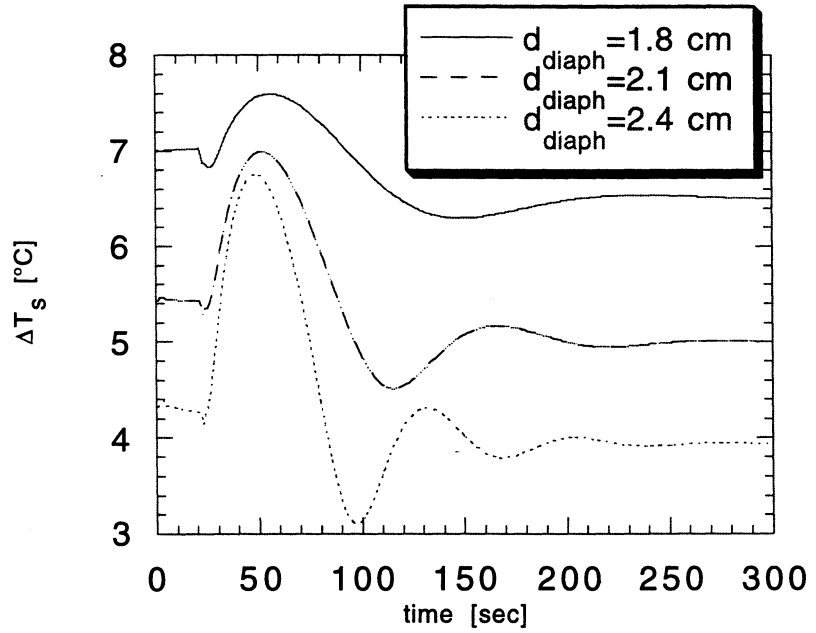

Figure 4.12 Superheat response for different diaphragm diameters following a step increase in suction-line pressure from 315 kPa to 324 kPa.

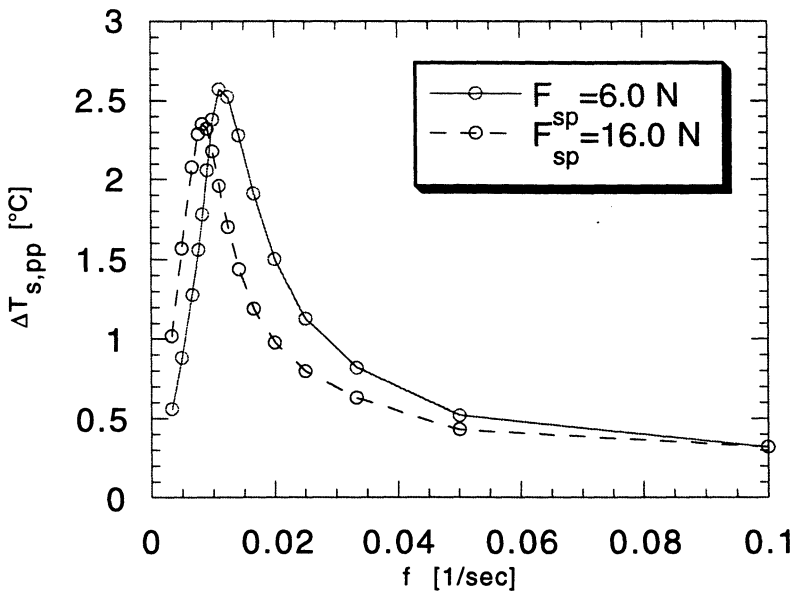

Figure 4.13 Peak-to-peak superheat response for different spring forces on a closed valve. Suction-line pressure is 315 kPa +/- 1%, perturbed at different frequencies.

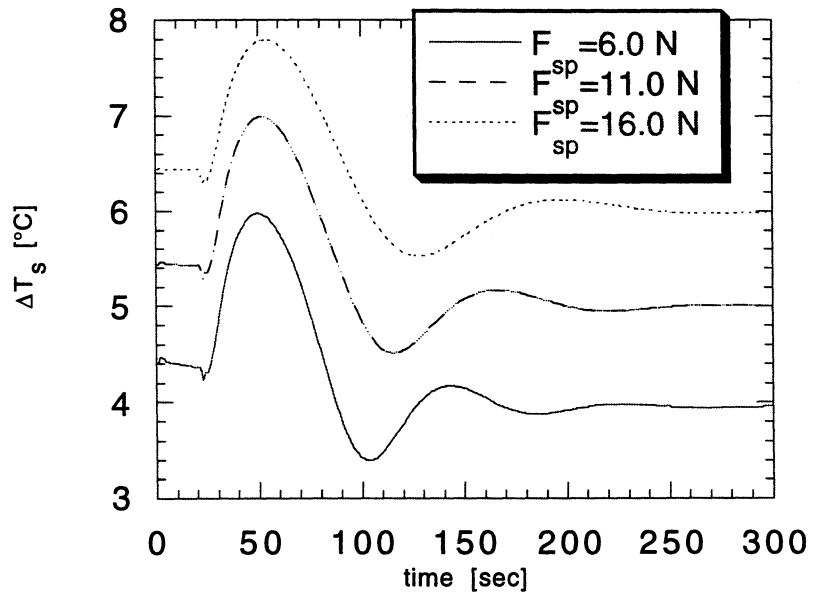

Figure 4.14 Superheat response for different spring forces on a closed valve following a step increase in suction-line pressure from 315 kPa to 324 kPa.

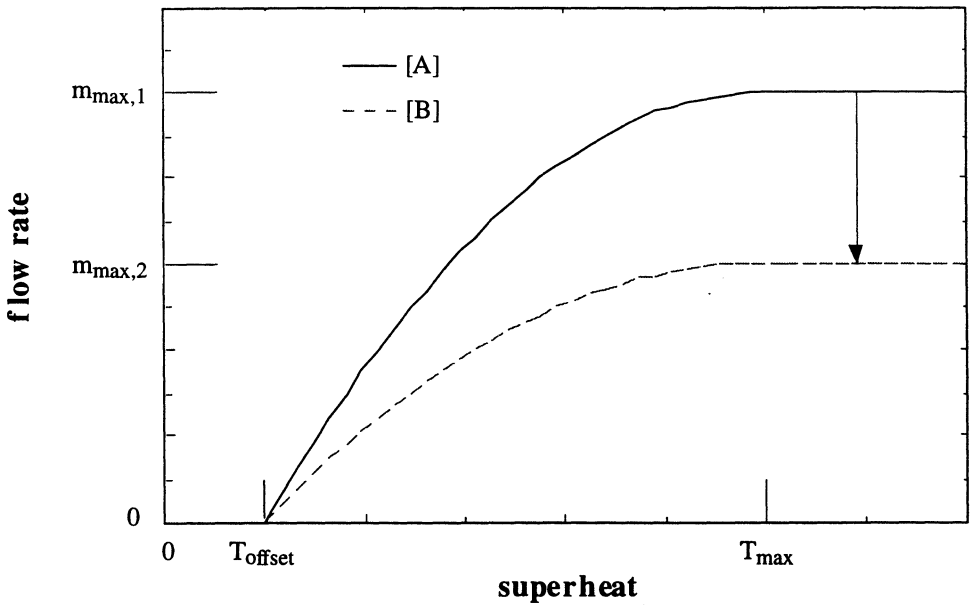

Figure 4.15 Flow rate versus superheat curves for two different sized thermostatic expansion valves. Decreasing the maximum flow rate stabilizes the performance of the valve.

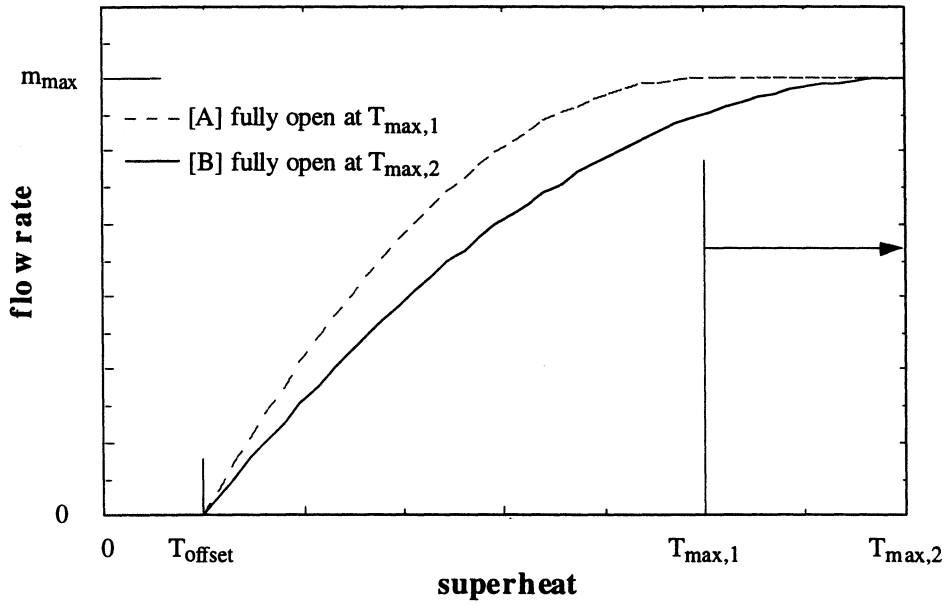

Figure 4.16 Flow rate versus superheat curves for two thermostatic expansion valves with different operating temperature ranges. Increasing the operating range of the valve by changing the spring constant or pin angle stabilizes the valve.

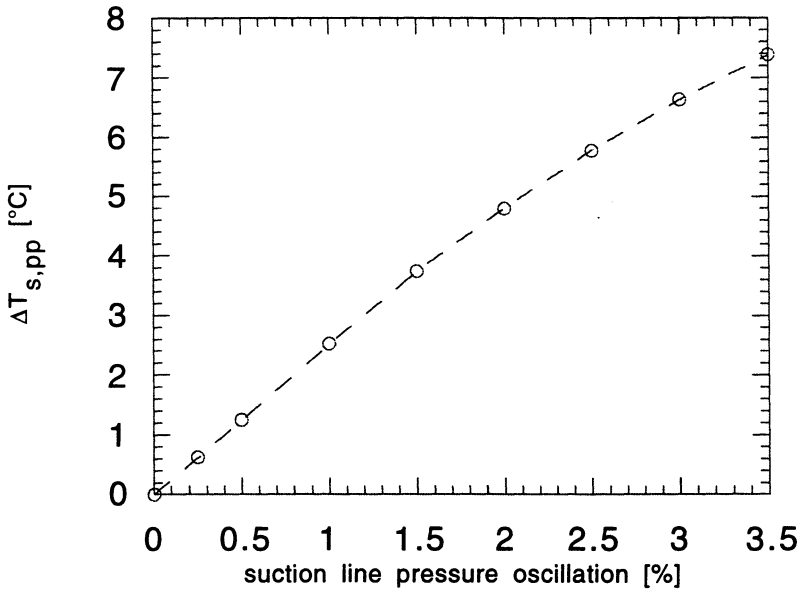

Figure 4.17 Effect of the magnitude of the suction-line pressure perturbation about 315 kPa on superheat fluctuations at a period of 80 seconds.

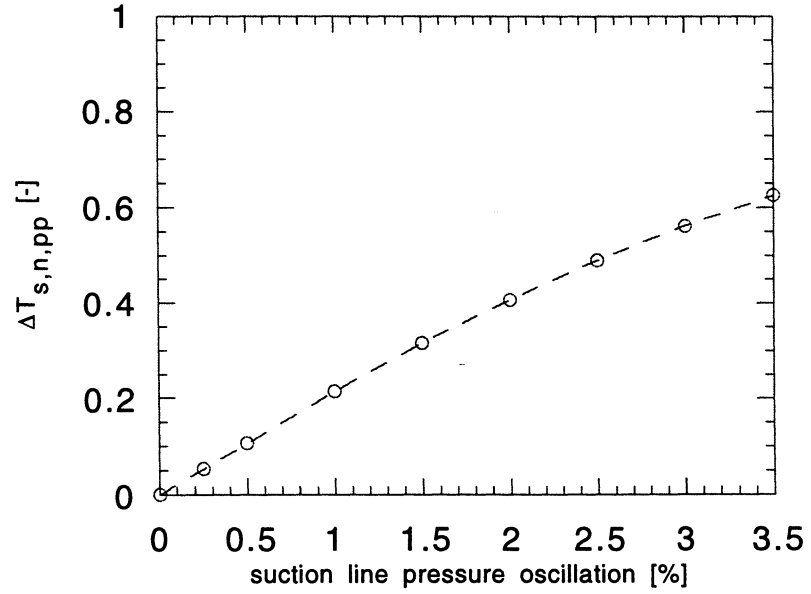

Figure 4.18 Effect of the magnitude of the suction-line pressure perturbation about 315 kPa on superheat fluctuations normalized by the maximum possible change ($T_{w,i}$ - T_{sat}).

CHAPTER 5 - CONCLUSION

This project utilized a mathematical model of a thermostatic expansion valve and concentric-tube heat exchanger to analyze evaporator dynamics and the superheat signal. The effects of different components in the thermostatic expansion valve were examined to determine their individual influence on the superheat signal for perturbations to the suction pressure. The contributions of this project can be summarized as follows.

Evaporator model

A two-passage, two-zone model of an evaporator has been developed based on the fundamental laws of conservation of mass, momentum and energy. This model is capable of simulating evaporator transients by using the two-phase flow length as a dynamic element. If the two-phase length exceeds the length of the evaporator, the mean void fraction becomes the dynamic element, from which the evaporator exit quality can be calculated. Maldistribution of flow among the evaporator passages is permitted by prescribing a quality ratio term, where this ratio allows the inlet quality into each passage to vary. The individual passage flow rates are determined as a function of the expansion valve opening and equalizing the pressure drop across the evaporator passages.

Thermostatic expansion valve model

A model of a thermostatic expansion valve has been developed that takes into account individual components of valve design, allowing for variation of parameters important to the valve operating behavior. Valve transients are modeled by using the bulb temperature as a dynamic element; the bulb temperature responds to both the evaporator exit temperature and the ambient air temperature. An orifice equation is used to calculate the maximum flow rate for the valve while the actual flow rate is calculated as a function of the deflection of a conical pin in relation to the orifice. Parameters included when modeling the

valve response include the orifice diameter, pin tip angle, spring constant, diaphragm area, bulb time constant, and the spring force exerted on a closed valve.

Superheat stability

Frequency response plots can be used to determine the effect of perturbations and design changes on the superheat signal. Simulations have shown that superheat instabilities are maximized within a critical range of frequencies during suction-line pressure oscillations. This critical band is for frequencies ranging from approximately 0.0083 to 0.025 Hz, depending on the valve characteristics. If superheat oscillations greater than a certain value are detrimental to the system, the frequency response plots will show the range of frequencies that are to be avoided. The magnitude of the superheat response is nearly linear with respect to the inlet disturbance, so the perturbation amplitude can and should be taken into account. The superheat response normalized by the maximum possible disturbance in the system can also be useful in understanding the relative size of the superheat fluctuations.

At high frequency suction-line pressure oscillations (to the far right of the superheat response peak), the superheat stability and flow rate are determined by valve parameters on the suction-line pressure side of the diaphragm: the orifice area, pin tip angle, spring constant, and diaphragm area. The slope of the flow rate versus superheat curve determines the magnitude of the superheat oscillations, where decreasing the slope minimizes the superheat response.

At low frequency suction-line pressure oscillations (to the far left of the superheat response peak), the superheat stability and flow rate are controlled by the speed at which the bulb responds to exit temperature fluctuations. In this region, the expansion valve is able to control superheat with feedback from the evaporator exit conditions, and the bulb time constant determines the frequency at which feedback begins to have an effect.

Suction-line pressure oscillations in the middle frequency ranges are affected by all valve parameters. Table 5.1 explains how the parameters can be adjusted to better control the superheat response. Changing the valve design to reduce the chance of hunting works in two ways. First, the magnitude of the superheat fluctuations to a pressure perturbation is minimized, as valve will be operating at the lower curves on the frequency response plots. Second, changing the valve parameters reduces superheat fluctuations by increasing the steady-state superheat. A higher average superheat signal reduces the chance for instabilities because the random behavior of two-phase flow may be damped out by the time the perturbations reach the evaporator exit.

Table 5.1 Means of increasing the superheat stability.

parameter	**to increase superheat stability:**	**frequency range**
bulb time constant	increase	low-middle
orifice area	decrease	middle-high
pin tip angle	decrease	middle-high
spring constant	increase	middle-high
diaphragm area	decrease	middle-high
initial spring force	increase	all

REFERENCES

1. Wang, H., and Touber, S., "Distributed and Non-Steady-State Modelling of an Air Cooler," *International Journal of Refrigeration*, 14, 98-111, 1991.

2. Stoecker, W.F., "Stability of an Evaporator-Expansion Valve Control Loop," *ASHRAE Transactions*, 72(2), IV.3.1-IV.3.8, 1966.

3. Broersen, P.M.T., and van der Jagt, M.F.G., "Hunting of Evaporators Controlled by a Thermostatic Expansion Valve," *Journal of Dynamic Systems, Measurement, and Control*, 102, 130-135, 1980.

4. He, X., Liu, S., and Asada, H., "Modeling of Vapor Compression Cycles for Multivariable Feedback Control of HVAC Systems," *Journal of Dynamic Systems, Measurement, and Control*, 119, 183-191, 1997.

5. de Bruijn, M., van der Jagt, M., and Machielsen, C., "Simulation Experiments of a Compression-Refrigeration System," *Proc. Proceedings IMACS Congress Simulation of System*, 645-653, 1979.

6. Dhar, M., and Soedel, W., "Transient Analysis of a Vapor Compression Refrigeration System: Part I - The Mathematical Model," *Proc. XVth International Congress of Refrigeration*, 1035-1048, 1979.

7. Grald, E., and MacArthur, J., "A Moving-Boundary Formulation for Modeling Time-Dependent Two-Phase Flows," *International Journal of Heat and Fluid Flow*, 13, 266-272, 1992.

8. Wedekind, G.L., and Kobus, C.J., "Modeling Thermally Governed Transient Flows in Multitube Evaporating Flow Systems With Thermal and Flow Distribution Asymmetry," *Journal of Heat Transfer*, 116, 503-505, 1994.

9. Jia, X., Tso, C.P., Chia, P.K., and Jolly, P., "A Distributed Model for Prediction of the Transient Response of an Evaporator," *International Journal of Refrigeration*, 18, 336-342, 1995.

10. Gruhle, W.D., and Isermann, R., "Modeling and Control of a Refrigerant Evaporator," *Journal of Dynamic Systems, Measurement, and Control*, 107, 235-240, 1985.

11. Nyers, J., and Stoyan, G., "A Dynamical Model Adequate for Controlling the Evaporator of a Heat Pump," *International Journal of Refrigeration*, 17, 101-108, 1994.

12. Yasuda, H., Touber, S., and Machielsen, C.H.M., "Simulation Model of a Vapor Compression Refrigeration System," *ASHRAE Transactions*, 89(2), 408-425, 1983.

13. Wedekind, G.L., *Transient Response of the Mixture-Vapor Transition Point in Two-Phase Horizontal Evaporating Flow*, Ph.D. Thesis, University of Illinois at Urbana-Champaign, 1965.

14. Mumma, S., *Predicting the Dynamic Response Charactaristics of a Refrigerant Evaporator*, M.S. Thesis, University of Illinois at Urbana-Champaign, 1971.

15. Tassou, S.A., and Al-Nizari, H.O., "Effect of Refrigerant Flow Control on the Thermodynamic Performances of Reciprocating Chillers," *Applied Energy*, 45, 101-116, 1993.

16. Hewitt, N.J., McMullan, J.T., and Moran, D.G., "The Control of a Refrigeration System Using a Compact Plate Heat Exchager as an Evaporator," *International Journal of Energy Research*, 17, 393-399, 1993.

17. Barnhart, J.S., *An Experimental Investigation of Flow Patterns and Liquid Entrainment in a Horizontal-Tube Evaporator*, Ph.D. Thesis, University of Illinois at Urbana-Champaign, 1992.

18. Najork, H., "Investigations on the Dynamical Behaviour of Evaporators with Thermostatic Expansion Valve," *Proc. XIII International Congress of Refrigeration*, 2, 759-769, 1971.

19. Schoen, A., "Resolving TEV Hunting Problems," *Heating/Piping/Air Conditioning*, 62, 69-72, 1990.

20. Lahey, R.T., Clause, A., and DiMarco, P., "Chaos and Non-Linear Dynamics of Density-Wave Instabilities in a Boiling Channel," *AIChE Symposium Series*, 256-261, 1989.

21. Lahey, R.T., and Podowski, M.Z.,"On the Analysis of Various Instabilities in Two-Phase Flows", in *Multiphase Science and Technology*, Hemisphere Publishing Corporation, 1989.

22. Yadigaroglu, G., and Chan, K.C.,"Analysis of Flow Instabilities", in *Two-Phase Flow Dynamics*, Hemisphere Publishing Corporation, 1981.

23. Bergles, A.E.,"Instabilities in Two-Phase Systems", in *Two-Phase Flow and Heat Transfer in the Power and Process Industries*, Hemisphere Publishing Corporation, 1981.

24. Boure, J.A., Bergles, A.E., and Tong, L.S., "Review of Two-Phase Flow Instability," *Nuclear Engineering and Design*, 25, 165-192, 1973.

25. Carey, V.,*Liquid-Vapor Phase-Change Phenomena*, Hemisphere Publishing Corporation, 1992.

26. Ledinegg, M., "Instability of Flow During Natural and Forced Circulation," *Die Warme*, 61, 891-898, 1938.

27. Incropera, F., and DeWitt, D.,*Fundamentals of Heat and Mass Transfer*, 4th ed., John Wiley & Sons, 1996.

28. de Souza, A., and Pimenta, M., "Prediction of Pressure Drop During Horizontal Two-Phase Flow of Pure and Mixed Refrigerants," *Proc. ASME Conference of Cavitation and Multiphase Flow*, 161-171, 1995.

29. Zivi, S. M., "Estimation of Steady-State Steam Void Fraction by Means of the Principle of Minimum Entropy Production," *Journal of Heat Transfer*, 86, 247-252, 1964.

30. Churchill, S., "Friction-Factor Equation Spans All Fluid-Flow Regimes," *Chemical Engineering*, 91-92, 1977.

31. Shah, M., "Chart Correlation for Saturated Boiling Heat Transfer: Equations and Further Study," *ASHRAE Transactions*, 88(1), 185-196, 1982.

32. Shah, M., "A New Correlation for Heat Transfer During Boiling Flow Through Pipes," *ASHRAE Transactions*, 82(2), 66-86, 1976.

33. Premoli, A., Francesco, D., and Prina, A., "An Empirical Correlation for Evaluating Two-Phase Mixture Density Under Adiabatic Conditions," *Proc. European Two-Phase Flow Group Meeting*, 1970.

34. Whalley, P.B.,*Boiling, Condensation and Gas-Liquid Flow*, Oxford University Press, New York, 1987.

35. Stegou-Sagia, A., "Properties of New Refrigerants and Predictions for Condensation Heat Transfer Enhancement with Low-Finned Tubes," *Energy*, 21, 1189-1199, 1996.

36. Hrnjak, P., Private communication; Work in progress, Singh, G., M.S. Thesis, University of Illinois at Urbana-Champaign, 1998.

37. ASHRAE,*ASHRAE Terminology of Heating, Ventilation, Air Conditioning, & Refrigeration*, American Society of Heating, Refrigerating, and Air-Conditioning Engineers, Inc., 1991.

38. Wedekind, G.L., Bhatt, B.L., and Beck, B.T., "A System Mean Void Fraction Model for Predicting Various Transient Phenomena Assosciated with Two-Phase Evaporating and Condensing Flows," *Int. J. Multiphase Flow*, 4, 97-114, 1978.

39. Liao, N.S., and Wang, C.C., "Analysis of Transient Flow Surge Phenomena in a Single Tube Condenser," *Int. Comm. Heat Mass Transfer*, 15, 257-268, 1988.

40. Gerald, Curtis F.,"Numerical Solution of Ordinary Differential Equations," in *Applied Numerical Analysis*, Addison-Wesley Publishing Co., 1985.

41. Wattelet, J., *Heat Transfer Flow Regimes of Refrigerants in a Horizontal-Tube Evaporator*, Ph.D. Thesis, University of Illinois at Urbana-Champaign, 1994.

APPENDIX A - MEAN VOID FRACTION THEORY

The evaporator model uses the mean void fraction theory in the two-phase regime [38]. The mean void fraction is used in a lumped parameter model and uncouples the transient momentum equation from the governing equations; made possible by assuming the mean void fraction is invariant with time.

The mean void fraction is found by Equation A.1, where the local void fraction is integrated over the two-phase region and then divided by the two-phase length. If the two-phase length has been normalized, Equation A.2 can be used instead.

$$\overline{\alpha}(t) \equiv \frac{1}{L_{tp}(t)} \int_{z=0}^{L_{tp}} \alpha(z,t)\, dz \qquad (A.1)$$

$$\overline{\alpha} = \int_{0}^{1} \alpha \cdot dL_n \qquad (A.2)$$

Wedekind proposed that the mean void fraction could be represented by a single dimensionless variable, ξ, thus eliminating the time dependence. Although representing the mean void fraction with ξ does not always allow for an exact solution, unacceptable errors are not produced. Experimental validation of the usefulness of the mean void fraction was initially produced by Wedekind [13] [38] and later verified by others [39]. The mean void fraction has been used in much of Wedekind's work as well as by other investigators [7] [4].

$$\xi \equiv \frac{z}{L_{tp}}$$

APPENDIX B - INTEGRATION TECHNIQUE

Several equations need to be integrated in space or time. For example, if the evaporator passage contains a superheat section the rate of change of the two-phase length is integrated in time; if there is no superheat section the rate of change of the mean void fraction is integrated in time. Also integrated in time is the rate of change of the thermostatic expansion valve bulb temperature. Even before calculating the evaporator transients, local variables such as the mean void fraction, average two-phase convection coefficient, and parameters for the two-phase pressure drop also need to be integrated over quality or length.

The integration technique used is the same in all cases. The first four steps in the numerical integration use Euler's method, shown in Equation B.1 for an integration in time. Euler's method is an approximation of a Taylor series expansion with an error on the order of the step size, either $O(\Delta t)$ or $O(\Delta L)$.

$$y_{n+1} = y_n + D_n \Delta t \tag{B.1}$$

where

$$D_n = \left.\frac{dy}{dt}\right)_n$$

After the first four steps the Adams method [40] is used for the integration, shown in Equation B.2. Adams is a multi-step method that makes use of information already known about the function and derivative in order to predict the next value, thereby increasing the accuracy to $O(\Delta t^4)$.

$$y_{n+1} = y_n + \frac{\Delta t}{24}\left(55\, D_n - 59\, D_{n-1} + 37\, D_{n-2} - 9\, D_{n-3}\right) \tag{B.2}$$

APPENDIX C - QUALITY DISTRIBUTION IN THE TWO-PHASE REGION

In order to find the average two-phase convection coefficient and mean void fraction, the local convection coefficient and void fraction are integrated over the length of two-phase region. However, the convection coefficient and void fraction correlations are a function of quality, not length. In many cases a linear relationship between quality and the length of the evaporating passage (uniform heat flux) is assumed to simplify the problem. This assumption is slightly inaccurate owing to the fact that the local convection coefficient changes in the two-phase region, therefore the rate at which the fluid evaporates changes as well.

From a specified quality increment and refrigerant flow rate, the heat rate can be found from Equation C.1; from which Equation C.2 can be used to calculate the change in water temperature. Because the water is in counterflow with the refrigerant, the water temperature along the evaporator is then found by prescribing the water exit temperature and integrating along the evaporator to the water inlet as shown in Equation C.3. Once the water temperature distribution is known, the surface area of the evaporator that is needed to increase the quality (dx) can be calculated from Equation C.4, and then the length of evaporator used is found from Equation C.5.

$$dq = m_r \lambda_{fg} dx \tag{C.1}$$

$$dT_w = \frac{dq}{m_w \cdot c} \tag{C.2}$$

$$T_w = T_{w,exit} + \int_{exit}^{inlet} dT_w \tag{C.3}$$

$$dA_{sur} = \frac{dq}{U_{tp} \cdot (T_w - T_r)} \tag{C.4}$$

$$dz = \frac{dA_{sur}}{\pi \cdot d} \tag{C.5}$$

where

$$U_{tp} = \frac{1}{\frac{1}{h_w} + \frac{1}{h_{r,local}}}$$

The actual quality distribution along a tube contrasted with the linear approximation assuming uniform heat flux is shown in Figure C.1. Examining how the evaporator increment changes for a constant change in quality helps give a better understanding of the error involved when assuming a uniform heat flux. Figure C.2 shows that the evaporator length increments range from 12 cm to 3 cm to produce a 1% increase in quality. This increment is constant when assuming a uniform heat flux, but clearly not the case here unless working only in the upper quality ranges; otherwise, the conditions at the exit of the evaporator are weighted more heavily than the conditions near the inlet of the evaporator.

Now it is obvious that the local quality through the evaporator needs to be known in order for correct integrals to be taken. It would be best to apply a curve fit to the quality variation over the two-phase length, but Figure C.3 shows that different convection coefficient correlations (Shah [31] and Wattelet [41]) produce different results. In an attempt to find a curve fit that is independent of the convection correlations the evaporating length was normalized, and better agreement is shown in Figure C.4.

An exponential curve fit in the form of Equation C.6 was used to approximate how the local evaporator quality varies over the two-phase length. The boundary condition for the quality at the evaporator inlet is the inlet quality, and at the end of the two-phase region the boundary condition is a quality of unity. Therefore, the exponential curve fit of quality is shown in Equation C.7. Figure 2.7 compares Equation C.7 to the quality distribution using Wattelet's correlation and it shows very good agreement.

$$y = C_1 \cdot e^{C_2 x} \tag{C.6}$$

B.C.: $\text{quality}\left(L_{tp} = 0\right) = x_{in}$

$\text{quality}\left(L_{tp} = 1\right) = 1$

Constants: $C_1 = x_{in}$

$$C_2 = \ln\left(\frac{1}{x_{in}}\right)$$

$$x_{local} = x_{in} \cdot \exp\left[\ln\left(\frac{1}{x_{in}}\right) \cdot \frac{L}{L_{tp}}\right] \qquad \text{(C.7)}$$

Now Equation C.7 can be used to correctly integrate the local convection coefficient and void fraction in order to find the average values in the two-phase region. Assumptions used in developing this correlation are that the refrigerant and water mass flow rates are known, and that a counterflow heat exchanger with water and R-134a was used.

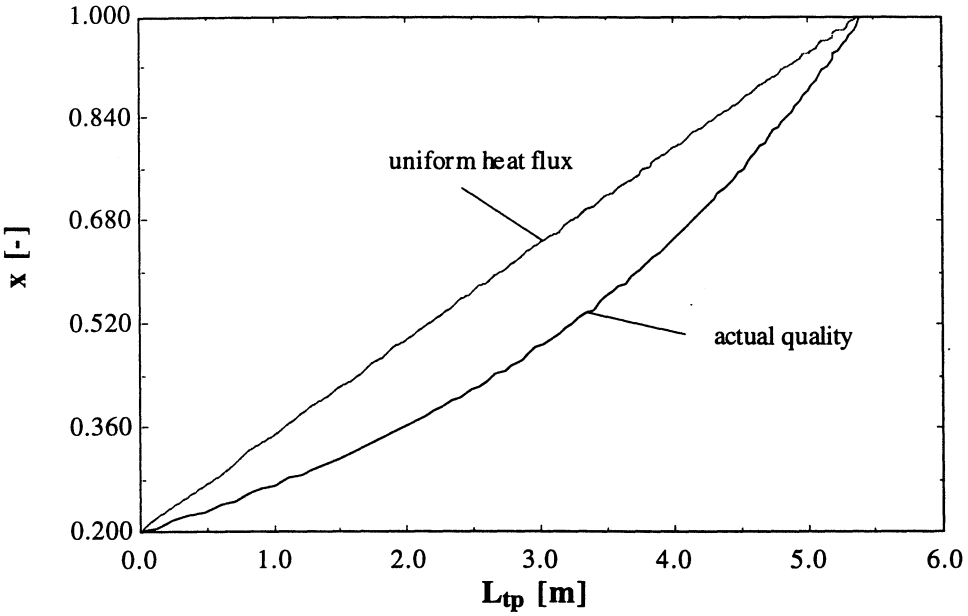

Figure C.1 Actual quality variation with length contrasted with the linear approximation that assumes a uniform heat flux

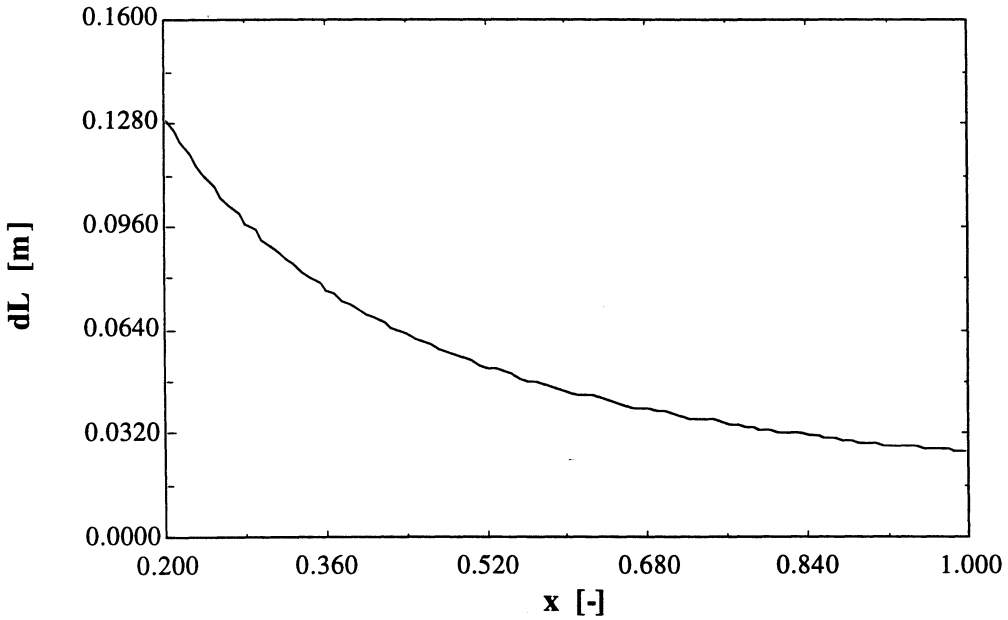

Figure C.2 Evaporator length increments needed for a 1% change in quality for a given evaporator geometry

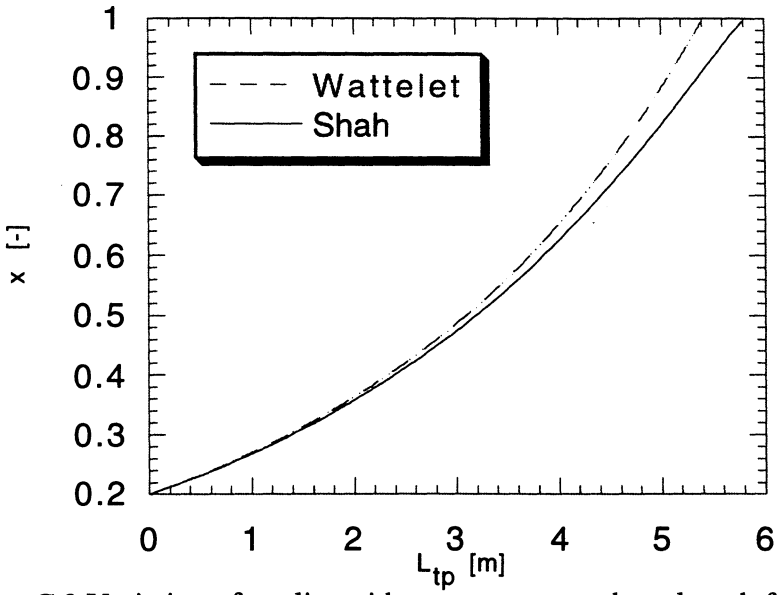

Figure C.3 Variation of quality with respect to two-phase length for both the Shah and Wattelet convection coefficient correlation

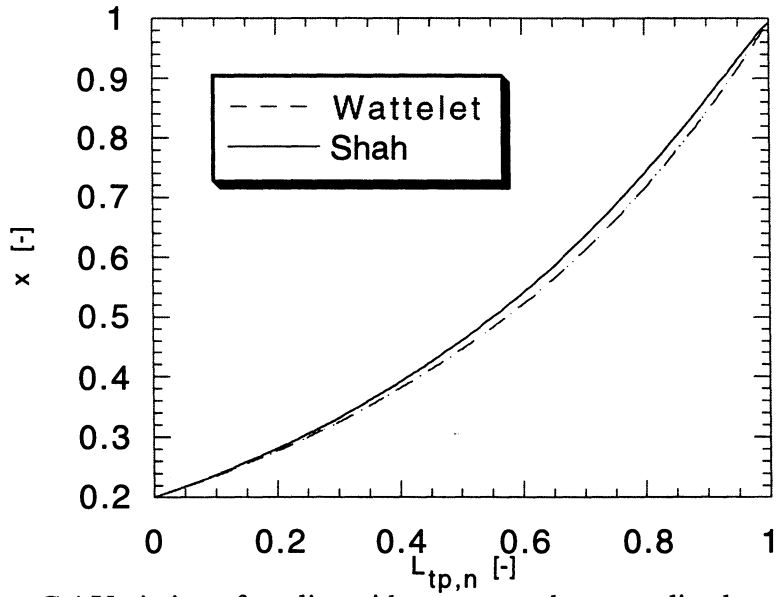

Figure C.4 Variation of quality with respect to the normalized two-phase length for both the Shah and Wattelet convection coefficient correlation

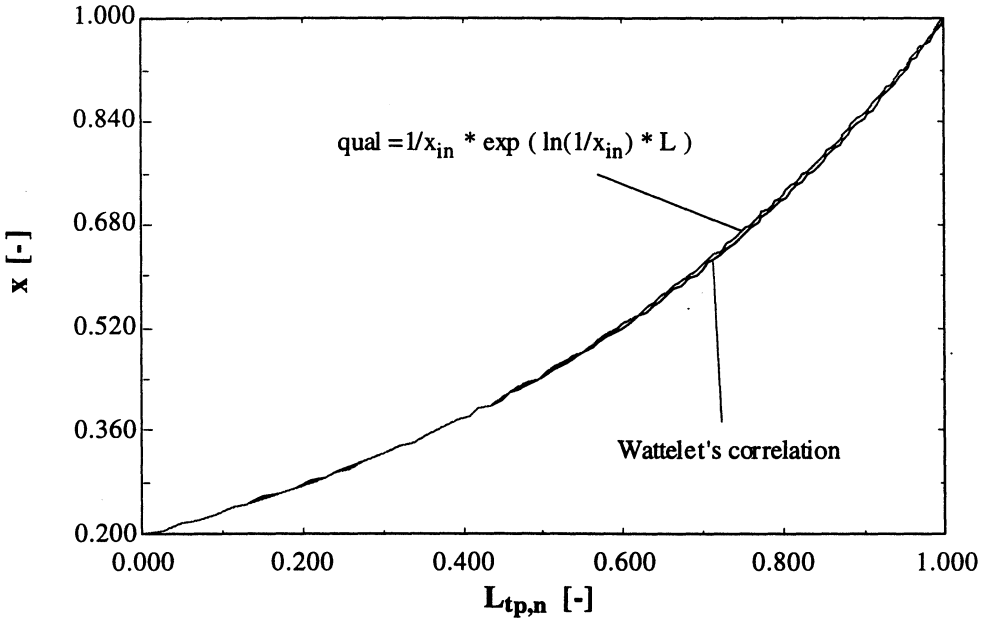

Figure C.5 Comparison of quality with respect to the normalized two-phase length for both the Wattelet convection coefficient and an exponential curve fit

APPENDIX D - SET OF COUPLED EQUATIONS USED FOR THE DYNAMIC MODELING OF AN EVAPORATOR

A set of non-linear algebraic equations coupled with ordinary differential equations is solved when modeling the dynamics of an evaporator. The equations are mainly composed of the conservation of mass, momentum, and energy. When there is evaporator superheat, the dynamic element in the model is the two-phase flow length; when there is liquid exiting the evaporator, the dynamic element is the mean void fraction. Different equation sets are needed for the cases when the evaporator has all passages superheated and for when liquid is exiting one evaporator passage.

The first equation set, titled "Newton Raphson Equations: Two Passages, includes superheat," is for the case when the evaporator consists of two flow passages, both of which have superheat. The second equation set, titled "Newton Raphson Equations: Two Passages, no superheat," is for a two-passage evaporator with liquid exiting one of the passages. The flow rate through the expansion valve, suction line pressure, and condenser pressure are all assumed to be known. During transient behavior it may be necessary for the simulation to switch between equation sets, depending on the evaporator conditions.

The equation sets are broken up into three sections. The first section lists the initial conditions that are known for the differential equations, and the third section lists those differential equations. The second section lists the algebraic equations that are solved simultaneously by a modified Newton-Raphson method.

The equation sets are also divided into eight columns. The first column lists the physical component or type of equation being solved; this is broken down into system equations, equations for each passage, equations for each of the two zones (superheat and two-phase), and then into the grouping of conservation equations. The second column then lists the equation being solved. Columns three and four list the known and unknown elements in the equation. Columns five and six are bookkeeping, keeping track of the

number of equations (#E) and number of unknowns (#U) in the system. Likewise, columns seven and eight are also bookkeeping, keeping track of the number of differential equations (DE) and initial conditions (IC) for the system.

Newton-Raphson Equations: Two Passages, includes superheat

COMPONENT	EQUATION	KNOWN	UNKNOWNS	#E	#U	IC	DE
2-Ph length	$L_{tp,1}(0) = L_{tp,1,i}$	$L_{tp,1,i}$	-----			1	-----
	$L_{tp,2}(0) = L_{tp,2,i}$	$L_{tp,2,i}$	-----			2	-----
System, General Equations							
header continuity	$m_{i,1} + m_{i,2} = m_{TXV}$	m_{TXV}	$m_{i,1}; m_{i,2}$	1	2		
flow rate	$m_{o,1} = G_{o,1} \cdot A_r \cdot 1000$	A_r	$m_{o,1}; G_{o,1}$	2	4		
	$m_{o,2} = G_{o,2} \cdot A_r \cdot 1000$	-----	$m_{o,2}; G_{o,2}$	3	6		
	$m_{i,1} = G_{i,1} \cdot A_r \cdot 1000$	-----	$G_{i,1}$	4	7		
	$m_{i,2} = G_{i,2} \cdot A_r \cdot 1000$	-----	$G_{i,2}$	5	8		
pressure drop	$\Delta P_{evap} = \Delta P_{s,1} + \Delta P_{acc,1} + \Delta P_{frict,1}$	-----	$\Delta P_{evap}; \Delta P_{s,1}$				
			$\Delta P_{frict,1}; \Delta P_{acc,1}$	6	12		
	$\Delta P_{evap} = \Delta P_{s,2} + \Delta P_{acc,2} + \Delta P_{frict,2}$	-----	$\Delta P_{s,2}; \Delta P_{frict,2}; \Delta P_{acc,2}$	7	15		
	$\Delta P_{TXV} = P_{cond} - P_{TXV}$	P_{cond}	$P_{TXV}; \Delta P_{TXV}$	8	17		
	$\Delta P_{evap} = P_{TXV} - P_{sl}$	P_{sl}	-----	9	17		
Tube 1: Two-Phase							
continuity	$m_{i,1} - m_{mid,1} = RHO_1 \cdot A_r \cdot \Psi_1$	RHO_1	$\Psi_1; m_{mid,1}$	10	19		
temp. difference	$\Delta T_{i,1} = T_{w,o,1} - T_{r,i}$	$T_{r,i}$	$\Delta T_{i,1}; T_{w,o,1}$	11	21		
	$\Delta T_{mid,1} = T_{w,mid,1} - T_{r,i}$	-----	$\Delta T_{mid,1}; T_{w,mid,1}$	12	23		
	$\Delta T_{LMTD,tp,1} = \frac{\Delta T_{i,1} - \Delta T_{mid,1}}{\ln\left(\frac{\Delta T_{i,1}}{\Delta T_{mid,1}}\right)}$	-----	$\Delta T_{LMTD,tp,1}$	13	24		
Energy	$E_{i,1} m_{i,1} + q_{tp,1} - i_v m_{mid,1} = ENGY_1 A_r \Psi_1$	$E_{i,1}; i_v; ENGY_1$	$q_{tp,1}$	14	25		
	$q_{tp,1} = m_{w,1} \cdot c_w \left(T_{w,mid,1} - T_{w,o,1}\right)$	$m_{w,1}; c_w$	-----	15	25		
	$q_{tp,1} = U_{tp,1} \cdot A_{sur,tp,1} \cdot \Delta T_{LMTD,tp,1}$	$A_{sur,tp,1}$	$U_{tp,1}$	16	26		
pressure drop	$\Delta P_{acc,1} = G_{i,1}^2 \left(out - in_1\right)$	$out; in_1$	-----	17	26		

	$\Delta P_{frict,1} = \left(\frac{\Delta P_{lo,1}}{1 - x_{i,1}}\right) \cdot \int \phi_{lo,1}{}^2 \cdot dx$	$x_{i,1}; \int \phi_{lo,1}{}^2$	$\Delta P_{lo,1}$	18	27
	$\Delta P_{lo,1} = 2 \cdot f_{lo,1} \cdot G_{i,1}{}^2 \cdot \frac{L_{tp,1}}{\rho_l \cdot d_r}$	$\rho_l; d_r$	$f_{lo,1}$	19	28
	$f_{lo,1} = \frac{0.079}{Re_{lo,1}{}^{0.25}}$	-----	$Re_{lo,1}$	20	29
	$Re_{lo,1} = \frac{G_{i,1} \cdot d_r}{\mu_l}$	μ_l	-----	21	29
Tube 1: Superheat					
continuity	$m_{mid,1} - m_{o,1} = -\rho_v \cdot A_r \cdot \Psi_1$	ρ_v	-----	22	29
temp. difference	$\Delta T_{o,1} = T_{w,i,1} - T_{r,o,1}$	$T_{w,i,1}$	$\Delta T_{o,1}; T_{r,o,1}$	23	31
	$\Delta T_{LMTD,s,1} = \frac{\Delta T_{mid,1} - \Delta T_{o,1}}{\ln\left(\frac{\Delta T_{mid,1}}{\Delta T_{o,1}}\right)}$	-----	$\Delta T_{LMTD,s,1}$	24	32
energy	$q_{s,1} = m_{w,1} \cdot c_w \left(T_{w,i,1} - T_{w,mid,1}\right)$	-----	$q_{s,1}$	25	33
	$q_{s,1} = m_{o,1} \cdot c_{r,v} \left(T_{r,o,1} - T_{r,i}\right)$	$c_{r,v}$	-----	26	33
	$q_{s,1} = U_{s,1} \cdot A_{sur,s,1} \cdot \Delta T_{LMTD,o,1}$	$A_{sur,s,1}$	$U_{s,1}$	27	34
	$U_{s,1} = \frac{1}{\frac{1}{h_{s,1}} + \frac{1}{h_w}}$	h_w	$h_{s,1}$	28	35
	$h_{s,1} = \frac{Nus_{s,1} \cdot k_v}{d_r}$	k_v	$Nus_{s,1}$	29	36
	$Nus_{s,1} = 0.023 \cdot Re_{s,1}{}^{0.8} \cdot Pr_s{}^{0.4}$	Pr_s	$Re_{s,1}$	30	37
pressure drop	$\Delta P_{s,1} = \left[f_{d,1}\left(\frac{L_{tot} - L_{tp,1}}{d_r}\right)\right] \frac{G_{o,1}{}^2}{2 \cdot \rho_v}$	-----	$f_{d,1}$	31	38
	$f_{d,1} = f\left(Re_{s,1}, \varepsilon\right)$	ε	-----	32	38

	$Re_{s,1} = \frac{G_{o,1} \cdot d_r}{\mu_v}$	μ_v	-----	33	38
Tube 2: Two-Phase					
continuity	$m_{i,2} - m_{mid,2} = RHO_2 \cdot A_r \cdot \Psi_2$	RHO_2	$\Psi_2; m_{mid,2}$	34	40
temp. difference	$\Delta T_{i,2} = T_{w,o,2} - T_{r,i}$	-----	$\Delta T_{i,2}; T_{w,o,2}$	35	42
	$\Delta T_{mid,2} = T_{w,mid,2} - T_{r,i}$	-----	$\Delta T_{mid,2}; T_{w,mid,2}$	36	44
	$\Delta T_{LMTD,tp,2} = \frac{\Delta T_{i,2} - \Delta T_{mid,2}}{\ln\left(\frac{\Delta T_{i,2}}{\Delta T_{mid,2}}\right)}$	-----	$\Delta T_{LMTD,tp,2}$	37	45
Energy	$E_{i,2} m_{i,2} + q_{tp,2} - i_v m_{mid,2} = ENGY_2 A_r \Psi_2$	$E_{i,2}; ENGY_2$	$q_{tp,2}$	38	46
	$q_{tp,2} = m_{w,2} \cdot c_w \cdot \left(T_{w,mid,2} - T_{w,o,2}\right)$	$m_{w,2}$	-----	39	46
	$q_{tp,2} = U_{tp,2} \cdot A_{sur,tp,2} \cdot \Delta T_{LMTD,tp,2}$	$A_{sur,tp,2}$	$U_{tp,2}$	40	47
pressure drop	$\Delta P_{acc,2} = G_{i,2}{}^2 (out - in_2)$	in_2	-----	41	47
	$\Delta P_{frict,2} = \left(\frac{\Delta P_{lo,2}}{1 - x_{i,2}}\right) \int \phi_{lo,2}{}^2 \cdot dx$	$x_{i,2}; \int \phi_{lo,2}{}^2$	$\Delta P_{lo,2}$	42	48
	$\Delta P_{lo,2} = 2 \cdot f_{lo,2} \cdot G_{i,2}{}^2 \cdot \frac{L_{tp,2}}{\rho_l \cdot d_r}$	-----	$f_{lo,2}$	43	49
	$f_{lo,2} = \frac{0.079}{Re_{lo,2}{}^{0.25}}$	-----	$Re_{lo,2}$	44	50
	$Re_{lo,2} = \frac{G_{i,2} \cdot d_r}{\mu_l}$	-----	-----	45	50
Tube 2: Superheat					
continuity	$m_{mid,2} - m_{o,2} = -\rho_v \cdot A_r \cdot \Psi_2$	-----	-----	46	50
temp. difference	$\Delta T_{o,2} = T_{w,i,2} - T_{r,o,2}$	$T_{w,i,2}$	$\Delta T_{o,2}; T_{r,o,2}$	47	52
	$\Delta T_{LMTD,s,2} = \frac{\Delta T_{mid,2} - \Delta T_{o,2}}{\ln\left(\frac{\Delta T_{mid,2}}{\Delta T_{o,2}}\right)}$	-----	$\Delta T_{LMTD,s,2}$	48	53

energy	$q_{s,2} = m_{w,2} \cdot c_w\left(T_{w,i,2} - T_{w,mid,2}\right)$	-----	$q_{s,2}$	49	54
	$q_{s,2} = m_{o,2} \cdot c_{r,v}\left(T_{r,o,2} - T_{r,i}\right)$	-----	-----	50	54
	$q_{s,2} = U_{s,2} \cdot A_{sur,s,2} \cdot \Delta T_{LMTD,s,2}$	$A_{sur,s,2}$	$U_{s,2}$	51	55
	$U_{s,2} = \frac{1}{\frac{1}{h_{s,2}} + \frac{1}{h_w}}$	-----	$h_{s,2}$	52	56
	$h_{s,2} = \frac{Nus_{s,2} \cdot k_v}{d_r}$	-----	$Nus_{s,2}$	53	57
	$Nus_{s,2} = 0.023 \cdot Re_{s,2}^{0.8} \cdot Pr_s^{0.4}$	-----	$Re_{s,2}$	54	58
pressure drop	$\Delta P_{s,2} = \left[f_{d,2}\left(\frac{L_{tot} - L_{tp,2}}{d_r} \right) \right] \frac{G_{o,2}^{\,2}}{2 \cdot \rho_v}$	$L_{tp,2}$	$f_{d,2}$	55	59
	$f_{d,2} = f\left(Re_{s,2}, \varepsilon\right)$	-----	-----	56	59
	$Re_{s,2} = \frac{G_{o,2} \cdot d_r}{\mu_v}$	-----	-----	57	59
overall convection	$U_{tp,1} = \frac{1}{\frac{1}{\bar{h}_{tp,1}} + \frac{1}{h_w}}$	-----	-----	58	59
	$U_{tp,2} = \frac{1}{\frac{1}{\bar{h}_{tp,2}} + \frac{1}{h_w}}$	-----	-----	59	59

Dynamic eqns	$\frac{dL_{tp,1}}{dt} = \Psi_1$	-----	1
	$\frac{dL_{tp,2}}{dt} = \Psi_2$	-----	2

Newton-Raphson Equations: Two Passages, no superheat

COMPONENT	EQUATION	KNOWN	UNKNOWNS	#E	#U	IC	DE
two-phase length	$L_{tp,1}(0) = L_{tp,1,i}$	$L_{tp,1,i}$	-----			1	-----
mean void fraction	$\overline{\alpha}_2(0) = \overline{\alpha}_{i,2}$	$\overline{\alpha}_{i,2}$	-----			2	-----
System, General Equations							
header continuity	$m_{i,1} + m_{i,2} = m_{TXV}$	m_{TXV}	$m_{i,1}; m_{i,2}$	1	2		
flow rate	$m_{o,1} = G_{o,1} \cdot A_r \cdot 1000$	A_r	$m_{o,1}; G_{o,1}$	2	4		
	$m_{o,2} = G_{o,2} \cdot A_r \cdot 1000$	-----	$m_{o,2}; G_{o,2}$	3	6		
	$m_{i,1} = G_{i,1} \cdot A_r \cdot 1000$	-----	$G_{i,1}$	4	7		
	$m_{i,2} = G_{i,2} \cdot A_r \cdot 1000$	-----	$G_{i,2}$	5	8		
pressure drop	$\Delta P_{evap} = \Delta P_{s,1} + \Delta P_{acc,1} + \Delta P_{frict,1}$	-----	$\Delta P_{evap}; \Delta P_{s,1}$				
			$\Delta P_{frict,1}; \Delta P_{acc,1}$	6	12		
	$\Delta P_{evap} = \Delta P_{acc,2} + \Delta P_{frict,2}$	-----	$\Delta P_{frict,2}; \Delta P_{acc,2}$	7	14		
	$\Delta P_{TXV} = P_{cond} - P_{TXV}$	P_{cond}	$P_{TXV}; \Delta P_{TXV}$	8	16		
	$\Delta P_{evap} = P_{TXV} - P_{sl}$	P_{sl}	-----	9	16		
Tube 1: Two-Phase							
continuity	$m_{i,1} - m_{mid,1} = RHO_1 \cdot A_r \cdot \Psi_1$	RHO_1	$\Psi_1; m_{tp,1}$	10	18		
temp. difference	$\Delta T_{i,1} = T_{w,o,1} - T_{r,i}$	$T_{r,i}$	$\Delta T_{i,1}; T_{w,o,1}$	11	20		
	$\Delta T_{mid,1} = T_{w,mid,1} - T_{r,i}$	-----	$\Delta T_{mid,1}; T_{w,mid,1}$	12	22		
	$\Delta T_{LMTD,tp,1} = \dfrac{\Delta T_{i,1} - \Delta T_{mid,1}}{\ln\left(\dfrac{\Delta T_{i,1}}{\Delta T_{mid,1}}\right)}$	-----	$\Delta T_{LMTD,tp,1}$	13	23		
energy	$E_{i,1} m_{i,1} + q_{tp,1} - i_v m_{tp,1} = ENGY_1 A_r \Psi_1$	$E_{i,1}; i_v; ENGY_1$	$q_{tp,1}$	14	24		
	$q_{tp,1} = m_{w,1} \cdot c_w \left(T_{w,mid,1} - T_{w,o,1}\right)$	$m_{w,1}; c_w$	-----	15	24		
	$q_{tp,1} = U_{tp,1} \cdot A_{sur,tp,1} \cdot \Delta T_{LMTD,tp,1}$	$A_{sur,tp,1}$	$U_{tp,1}$	16	25		
pressure drop	$\Delta P_{acc,1} = G_{i,1}^2 \left(out - in_1\right)$	$out; in_1$	-----	17	25		

	$\Delta P_{frict,1} = \left(\frac{\Delta P_{lo,1}}{1 - x_{i,1}}\right) \int \phi_{lo,1}^{\ 2} \cdot dx$	$x_{i,1}; \int \phi_{lo,1}^{\ 2}$	$\Delta P_{lo,1}$	18	26
	$\Delta P_{lo,1} = 2 \cdot f_{lo,1} \cdot G_{i,1}^{\ 2} \cdot \frac{L_{tp,1}}{\rho_l \cdot d_r}$	$\rho_l; d_r$	$f_{lo,1}$	19	27
	$f_{lo,1} = \frac{0.079}{Re_{lo,1}^{\ 0.25}}$	-----	$Re_{lo,1}$	20	28
	$Re_{lo,1} = \frac{G_{i,1} \cdot d_r}{\mu_l}$	μ_l	-----	21	28
Tube 1: Superheat					
continuity	$m_{mid,1} - m_{o,1} = -\rho_v \cdot A_r \cdot \Psi_1$	ρ_v	-----	22	28
temp. difference	$\Delta T_{o,1} = T_{w,i,1} - T_{r,o,1}$	$T_{w,i,1}$	$\Delta T_{o,1}; T_{r,o,1}$	23	30
	$\Delta T_{LMTD,s,1} = \frac{\Delta T_{mid,1} - \Delta T_{o,1}}{\ln\left(\frac{\Delta T_{mid,1}}{\Delta T_{o,1}}\right)}$	-----	$\Delta T_{LMTD,s,1}$	24	31
energy	$q_{s,1} = m_{w,1} \cdot c_w \left(T_{w,i,1} - T_{w,mid,1}\right)$	-----	$q_{s,1}$	25	32
	$q_{s,1} = m_{o,1} \cdot c_{r,v} \left(T_{r,o,1} - T_{r,i}\right)$	$c_{r,v}$	-----	26	32
	$q_{s,1} = U_{s,1} \cdot A_{sur,s,1} \cdot \Delta T_{LMTD,s,1}$	$A_{sur,s,1}$	$U_{s,1}$	27	33
	$U_{s,1} = \frac{1}{\frac{1}{h_{s,1}} + \frac{1}{h_w}}$	h_w	$h_{s,1}$	28	34
	$h_{s,1} = \frac{Nus_{s,1} \cdot k_v}{d_r}$	k_v	$Nus_{s,1}$	29	35
	$Nus_{s,1} = 0.023 \cdot Re_{s,1}^{\ 0.8} \cdot Pr_s^{\ 0.4}$	Pr_s	$Re_{s,1}$	30	36
pressure drop	$\Delta P_{s,1} = \left[f_{d,1}\left(\frac{L_{tot} - L_{tp,1}}{d}\right)\right] \frac{G_{o,1}^{\ 2}}{2 \cdot \rho_v}$	-----	$f_{d,1}$	31	37
	$f_{d,1} = f\left(Re_{s,1}; \varepsilon\right)$	ε	-----	32	37

	$Re_{s,1} = \frac{G_{o,1} \cdot d_r}{\mu_v}$	μ_v	-----	33	37

Tube 2: Two-Phase

continuity	$m_{i,2} - m_{o,2} = A_r \cdot L_{tot}(\rho_v - \rho_l)\Lambda$	-----	Λ	34	38
temp. difference	$\Delta T_{i,2} = T_{w,o,2} - T_{r,i}$	-----	$\Delta T_{i,2}; T_{w,o,2}$	35	40
	$\Delta T_{o,2} = T_{w,i,2} - T_{r,i}$	$T_{w,i,2}$	$\Delta T_{o,2}$	36	41
	$\Delta T_{LMTD,tp,2} = \frac{\Delta T_{i,2} - \Delta T_{o,2}}{\ln\left(\frac{\Delta T_{i,2}}{\Delta T_{o,2}}\right)}$	-----	$\Delta T_{LMTD,tp,2}$	37	42
energy	$E_{i,2}m_{i,2} + q_{tp,2} - \left(i_l + x_{o,2}\lambda_{fg}\right)m_{o,2} = A_r \cdot L_{tot}(h_v\rho_v - h_l\rho_l)\Lambda$				
		$x_{o,2}$	$q_{tp,2}$	38	43
	$q_{tp,2} = m_{w,2} \cdot c_w\left(T_{w,i,2} - T_{w,o,2}\right)$	$m_{w,2}$	-----	39	43
	$q_{tp,2} = U_{tp,2} \cdot A_{sur,tp,2} \cdot \Delta T_{LMTD,tp,2}$	$A_{sur,tp,2}$	$U_{tp,2}$	40	44
pressure drop	$\Delta P_{acc,2} = G_{i,2}{}^2(out - in_2)$	in_2	-----	41	44
	$\Delta P_{frict,2} = \left(\frac{\Delta P_{lo,2}}{x_{o,2} - x_{i,2}}\right)\int \phi_{lo,2}{}^2 \cdot dx$	$x_{i,2}; \int \phi_{lo,2}{}^2$	$\Delta P_{lo,2}$	42	45
	$\Delta P_{lo,2} = 2 \cdot f_{lo,2} \cdot G_{i,2}{}^2 \cdot \frac{L_{tot}}{\rho_l \cdot d_r}$	-----	$f_{lo,2}$	43	46
	$f_{lo,2} = \frac{0.079}{Re_{lo,2}{}^{0.25}}$	-----	$Re_{lo,2}$	44	47
	$Re_{lo,2} = \frac{G_{i,2} \cdot d_r}{\mu_l}$	-----	-----	45	47
overall convection	$U_{tp,1} = \frac{1}{\frac{1}{\bar{h}_{tp,1}} + \frac{1}{h_w}}$	-----	-----	46	47

	$U_{tp,2} = \frac{1}{\frac{1}{\bar{h}_{tp,2}} + \frac{1}{h_w}}$	-----	-----	47	47
two-phase length	$\frac{dL_{tp,1}}{dt} = \Psi_1$			-----	1
mean void fraction	$\frac{d\bar{\alpha}_2}{dt} = \Lambda$			-----	2